

MAR 2 1962

Lewis

[Handwritten initials]

AD-B186 301



COPY 1

103,276

NASA-8

REPORT
ARC - R - 30

A THEORY AND APPLICATIONS
OF FILAMENTARY STRUCTURES

PART ONE: THEORETICAL STUDIES

DTIC USER ONLY

DTIC
SELECTE
JUL 2 1994
S B D

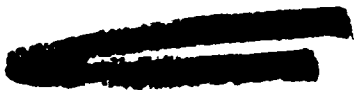


2280

94-19187



V-103,276
Part I



ASTRO

**RESEARCH
CORPORATION**

SANTA BARBARA, CALIFORNIA

94 6 22 002

Copy _____ of _____
Series _____

REPORT

ARC - R - 30

A THEORY AND APPLICATIONS
OF FILAMENTARY STRUCTURES

PART ONE: THEORETICAL STUDIES

SUBMITTED UNDER CONTRACT NASr - 8

PREPARED BY:
H. U. SCHUERCH
O. R. BURGGRAF
A. C. KYSER

DATE: September 30, 1961

APPROVED BY:

H. U. Schuerch
H. U. SCHUERCH

DTIC QUALITY INSPECTED 2

ASTRO RESEARCH CORPORATION
P. O. BOX 4128
Santa Barbara, California
Telephone: Woodland 6-6005

INDEX

	SUMMARY - - - - -	iii
	LIST OF SYMBOLS - - - - -	iv
I.	INTRODUCTION- - - - -	1
II.	THEORY OF MONOTROPIC MEMBRANES - - - - -	3
	A. Definitions - - - - -	3
	B. Geometry of Monotropic Membranes - - - - -	4
	C. Equilibrium Condition - - - - -	7
	D. Discussion - - - - -	8
III.	ISOTENSOID PRESSURE SHELLS OF REVOLUTION - - - - -	10
	A. Basic Equations - - - - -	10
	B. Methods of Solution- - - - -	14
	C. Discussion of Results - - - - -	16
IV.	MORPHOLOGY OF CLOSED PRESSURE VESSELS - - - - -	21
	A. Containers with Simply Connected Volume - - - - -	21
	B. Containers with Doubly Connected Volume - - - - -	23
V.	CONCLUDING REMARKS - - - - -	26
	A. Structural Weights, Enclosed Volumes and Surface Areas of Isotensoid Pressure Vessels - - - - -	26
	B. Periodicity of Winding Patterns - - - - -	27
	C. Instability Phenomena in Toroidal Pressure Vessels - - - - -	27
	D. Non-Monotropic Filamentary Textures - - - - -	28
	E. Isotensoid, Pressure Stabilized Structures Subject to Concentrated Loads - - - - -	29
	REFERENCES - - - - -	31
	APPENDIX A - - - - -	33
	APPENDIX B - - - - -	36
	FIGURES - - - - -	39 -66

SUMMARY

A general theory of filamentary structures consisting of monotropic membranes is presented. Applications to isotensoid pressure vessels with rotational symmetry demonstrate the use of the general theory. Particular attention is given to applications of filamentary design of variable-geometry expandable structures.

An extension of the theory to pressurized filamentary structures subject to centrifugal loading and the special case of meridional winding patterns are presented in two Appendices.

Physical interpretation of the resulting shapes and winding patterns leads to a discussion of the morphology of filament-wound pressure vessels.

Design implications in terms of weight/volume/pressure and volume/surface-area relations are discussed. Directions of further investigations are indicated, involving studies of instability phenomena, development of filamentary textures other than those described by monotropic membranes, and design for concentrated-load-carrying pressure-stabilized structures.

Accession For	
NTIS GRA&I	<input type="checkbox"/>
DTIC TAB	<input checked="" type="checkbox"/>
Unannounced	<input type="checkbox"/>
Justification	
By _____	
Distribution/	
Availability Codes	
Dist	Avail. and/or Special
12	

LIST OF SYMBOLS

C	:	Fiber helix parameter
EI	:	Bending stiffness of analog column
$E_I G_I$:	Coefficients of the first fundamental form
$E_{II} G_{II}$:	Coefficients of the second fundamental form
\mathcal{E}	:	Elliptical integral of the second kind
F	:	Force/unit length
\mathcal{F}	:	Elliptical integral of the first kind
K	:	Pressure load parameter
N_i	:	Fraction of filament count
P	:	Load, (also used as "point on surface")
R	:	Non-dimensional radial coordinate
S	:	Surface area
(SF)	:	Safety factor
T	:	Fiber force
V	:	Volume
\bar{X}	:	Radius vector
Z	:	Non-dimensional axial coordinate
\bar{e}	:	Unit vector
h	:	Distance between poles
i	:	Integer
k	:	Curvature
λ	:	Argument of elliptical integral
l	:	Specific strength
n	:	Number of filaments (fiber count)
m'	:	Mass/unit length
p	:	Pressure
r	:	Radius
s	:	Arc length

LIST OF SYMBOLS (Continued)

u, v	:	Curvilinear coordinates
x, y, z	:	Cartesian coordinates
Ω	:	Centrifugal load parameter
α	:	Slope of meridian
β	:	Helix angle
θ	:	Central angle of fiber spacing
ϕ	:	Central angle
ρ	:	Radius of curvature
ω	:	Angular velocity
ξ	:	Integration variable

I. INTRODUCTION

A review of recent developments in the field of advanced structures for aeronautical, missile-borne, and space applications shows an increasing interest in exploiting the remarkable physical-mechanical properties of fibered materials. A large volume of published information (See, for instance, Refs. 8, 9, 15, and 16) is available, particularly in the field of filament wound structures. The attraction of filamentary structures may be found in three areas:

- (1) Considerably higher strength/weight ratios are potentially possible (and have, in certain instances, been demonstrated) by use of filamentary materials as compared to similar structures made from conventional isotropic material (Ref. 21).
- (2) The potential of obtaining relative insensitivity to crack-propagation due to accidental damage in filamentary arrays typical for filament-wound structures has been shown theoretically by Hedgepeth (Ref. 17). Furthermore, tests on single fibers of many materials show increased strength and resistance to elevated temperature (Ref. 18), creep, and fatigue as compared to the properties of the same materials in bulk form. Realization of the implied potential performance gains depends upon proper utilization of fibers (isotensoid design, Ref. 19) and remains to be generally demonstrated in practice.
- (3) The peculiar, non-isotropic character of filamentary textured material may be used to advantage in specific applications. One of particular interest is the design of expandable structures with variable geometry, for which a multitude of space applications are presently considered.

There exists a need for a fundamental approach to the problem of design synthesis of filamentary structures. The present report deals with a specific and relatively important species of filamentary structures, namely those pro-

duced by filament-winding processes, both from the point of view of developing a basic understanding, and from the point of view of particular applications to toroidal pressure containers.

II. THEORY OF MONOTROPIC MEMBRANES

A. Definitions

Consider a thin walled shell made from a material which consists of an array of filaments (Figure 1, page 39). The thickness of the shell may be variable, but will always be sufficiently small so that the geometrical properties of the shell can be described by its middle surface (membrane).

Consider now a small but finite domain of this shell. The geometrical arrangement of the filaments traversing this domain shall be such that the tangents to all filaments have a uniquely determined direction, described by an angle β between the filament centerlines and a coordinate line inscribed on the membrane surface. The centerlines of all filaments, thus, belong to a "one parametric" family of curves. Mathematically, this can be expressed by

$$\beta = \beta_{(u, v)} \quad (1)$$

where u and v are surface coordinates and $\beta_{(u, v)}$ is a unique and continuous function of the surface coordinates u and v . The condition of uniquely defined filament direction shall hold for all regular points of the membrane, but may not hold for points of singularity such as poles, lines of cross-over, etc.

We will assume that the filaments are completely flexible and capable of carrying only normal forces only in the direction β of their local tangents. If these filaments are bonded together by a matrix material, we will consider this matrix to be completely compliant. Thus, the only stresses that can exist in this shell are normal stresses in the locally defined direction β .

A structure of this nature shall be called a Monotropic Membrane, to indicate the unique and predetermined character of stress distribution.

Filament-wound structures can frequently be considered as combinations of contiguous or intermeshing monotropic membranes. This is particularly

true if the filaments are relatively rigid and the matrix or binder material is relatively flexible, so that the predominant part of the structural loading is carried by the filamentary constituent of the composite material.

B. Geometry of Monotropic Membranes

In this paragraph, geometrical relations referring to surfaces and curves on surfaces are summarized from Refs. 1 through 3 for convenience of the subsequent discussion of the properties of monotropic membranes.

Consider the middle surface of the shell described by a vector \bar{X} extending from an arbitrary origin "O" to any point "P" on the surface (Figure 2a, page 40). The surface is inscribed with a system of orthogonal curvilinear coordinates u, v . For the purpose of this discussion, the lines $u = \text{const}$ and $v = \text{const}$ will be chosen as the lines of principal curvature of the surface.

Let $(\bar{e}_t, \bar{e}_n, \bar{e}_g)$ be a triad of mutually orthogonal unit vectors, moving along the centerline of a filament located on the surface where

\bar{e}_t is tangential to the filament centerline.

\bar{e}_n is perpendicular to the surface.

\bar{e}_g is located in the tangent plane to the surface centerline and normal to the filament tangent.

The rate of change of the unit tangent vector \bar{e}_t , while proceeding along the filament centerline for a differential length ds , is equal to the curvature vector:

$$\bar{k} = \frac{d\bar{e}_t}{ds} \quad (2)$$

where \bar{k} is a vector collinear with the radius vector of curvature $\bar{\rho}$ and of absolute magnitude $\frac{1}{\bar{\rho}}$.

The normal curvature vector \bar{k}_n is the projection of \bar{k} into a plane spanned by \bar{e}_t and \bar{e}_n . Its magnitude, the normal curvature, can be expressed by the scalar vector product

$$k_n = (\bar{k} \cdot \bar{e}_n) \quad (3)$$

The geodesic curvature vector \bar{k}_g is the projection of \bar{k} into the tangent plane to the surface. Its magnitude, the geodesic curvature, can be expressed by the scalar vector product

$$k_g = (\bar{k} \cdot \bar{e}_g) \quad (4)$$

Curves of vanishing geodesic curvature are called geodesics. They have the characteristics of straight lines in the non-Euclidian geometry of the surface described by \bar{X} . Thus, they are also curves of minimum (or maximum) distance between two points on the surface. A particularly important characteristic of geodesics is the fact that geodesics retain their geodesic character during an inextensional (bending) deformation of the membrane.

The pertinent geometrical properties of the surface can be expressed in terms of two fundamental quadratic forms:

- (1) The first fundamental form describes the length ds of a line element on the surface. For an orthogonal surface coordinate system (u, v) this first fundamental form reduces to

$$(ds)^2 = (d\bar{X} \cdot d\bar{X}) = E_I du^2 + G_I dv^2 \quad (5)$$

where

$$E_I = \left(\frac{\partial \bar{X}}{\partial u} \cdot \frac{\partial \bar{X}}{\partial u} \right)$$

$$G_I = \left(\frac{\partial \bar{X}}{\partial v} \cdot \frac{\partial \bar{X}}{\partial v} \right)$$

- (2) The second fundamental form is a measure of the change of the surface tangent plane or surface normal vector, i. e., a measure for the curvature and twist of the surface. For orthogonal coordinate systems, the second fundamental form reduces to

$$- (d\bar{X} \cdot d\bar{e}_n) = E_{II} du^2 + G_{II} dv^2$$

where

$$E_{II} = \left(\frac{\partial^2 \bar{X}}{\partial u^2} \cdot \bar{e}_n \right)$$

$$G_{II} = \left(\frac{\partial^2 \bar{X}}{\partial v^2} \cdot \bar{e}_n \right)$$

Now let $k_{n(v)}$ and $k_{g(v)}$ be the normal and geodesic curvature of the lines $v = \text{const}$, and let $k_{n(u)}$ and $k_{g(u)}$ be the normal and geodesic curvature of the lines $u = \text{const}$.

The normal curvature of the filament centerline forming an angle β with the line $v = \text{const}$ is then given by Euler's Theorem for the orthogonal system of surface coordinates formed by the lines of principal curvature:

$$k_{n(\beta)} = k_{n(v)} \cos^2 \beta + k_{n(u)} \sin^2 \beta \quad (7)$$

The geodesic curvature of the filament centerline forming an angle β with the line $v = \text{const}$ is given by Liouville's Theorem for any orthogonal system of surface coordinates:

$$k_{g(\beta)} = \frac{d\beta}{ds} + k_{g(v)} \cos \beta + k_{g(u)} \sin \beta \quad (8)$$

Finally, the normal and geodesic curvatures of the coordinate lines are related to the coefficients of the first and second fundamental forms of Eq. 5 and 6 as follows:

$$\left. \begin{aligned} k_{n(v)} &= \frac{E_{II}}{E_I} \\ k_{n(u)} &= \frac{G_{II}}{G_I} \end{aligned} \right\} \quad (9)$$

$$\left. \begin{aligned} k_{g(v)} &= -\frac{\partial E_I}{\partial v} \frac{1}{2E_I \sqrt{G_I}} \\ k_{g(u)} &= \frac{\partial G_I}{\partial u} \frac{1}{2G_I \sqrt{E_I}} \end{aligned} \right\} \quad (10)$$

C. Equilibrium Condition

Consider an element of a filament of length ds . subject to an axial force vector T and an external force vector/unit length F' of arbitrary direction (Figure 3, page 41). Equilibrium for the element demands that

$$\bar{T}_{(s+ds)} - \bar{T}_{(s)} + \bar{F}'_{(s)} ds = 0$$

or, in differential vector form

$$\frac{d\bar{T}_{(s)}}{ds} + \bar{F}'_s = 0 \quad (11)$$

The vector $\bar{T}_{(s)}$ can be written as $\bar{T}_{(s)} = \bar{e}_t \cdot T_{(s)}$, where $T_{(s)}$ is the magnitude of the force vector \bar{T} at s . Thus, Eq. (11) can be written as

$$\frac{d}{ds} (T_{(s)} \cdot \bar{e}_t) + \bar{F}' = 0$$

and by partial differentiation of the first term, considering Eq. (2) we obtain

$$\frac{dT_{(s)}}{ds} \bar{e}_t + T_{(s)} \bar{k} + \bar{F}'_{(s)} = 0 \quad (12)$$

Scalar multiplication of (12) in turn with the three unit vectors of the triad ($\bar{e}_t, \bar{e}_n, \bar{e}_g$) yields three scalar equilibrium conditions:

$$\frac{dT}{ds} + F'_t = 0 \quad (13)$$

$$Tk_n + F'_n = 0 \quad (14)$$

$$Tk_g + F'_g = 0 \quad (15)$$

where

$$F'_t = (\bar{F}' \cdot \bar{e}_t)$$

$$F'_n = (\bar{F}' \cdot \bar{e}_n)$$

$$F'_g = (\bar{F}' \cdot \bar{e}_g)$$

are the three components of the external load vector in the three directions indicated by the triad $(\bar{e}_t, \bar{e}_n, \bar{e}_g)$, respectively (Figure 3, page 26).

D. Discussion

The equations (13) through (15) relate the filament load to the geometrical characteristics of the filament given by \bar{e}_t , k_n , and k_g . The two curvatures are related to the properties of the lines of principal curvature serving as surface coordinates by Euler's and Liouville's Theorem (7) and (8), respectively, and may be related to the coefficients of the fundamental forms as given in (9) and (10).

An examination of the equilibrium equations (13) through (15) yields the following results:

- (1) For a given monotropic shell, only one of the three components of external load vector \bar{F}' can be freely chosen, while still satisfying all conditions of equilibrium. This implies that the monotropic shell is two-fold statically underdeterminate, i. e., it will act as a mechanism rather than as a structure under all external loads not satisfying conditions (13) through (15). This effect may be beneficial where a "variable geometry structure" such as a foldable and expandable shell is desired. On the other hand, however, peculiar instability phenomena, as discussed in the latter portion of this report, may occur requiring particular study and attention.

In general, it is necessary to have three contiguous or intermeshing layers of monotropic membranes present in a structural shell in order to produce a statically determinate system.

(2) For the case where $F'_t = 0$, the fiber force T is invariant throughout the structure. Such a structure is called "Isotensoid" (from iso-equal, tensus-extension) to indicate the uniform character of stress and strain in the load carrying material (Ref. 8 and 19). An isotensoid structure, furthermore, constitutes an optimum design, since the material will be stressed equally (i. e. , utilized uniformly) at all points.

(3) For monotropic shells that are loaded by pressure loads normal to the surface, both F'_t and F'_g vanish. The structure is isotensoid and the geodesic curvature k_g of the filaments vanishes; therefore, the curves of filament centerlines describe geodesics of the membrane surface. These are of particular importance for the case of filament winding, since a fiber placed under some tension on an arbitrarily shaped mandrel will tend to follow a geodesic on the mandrel surface.

The general problem of optimum isotensoid design synthesis for a filament-wound structure may now be stated as follows:

For a given external load, find the surface shape and associated filamentary geometry of one or several monotropic membranes for which F'_t vanishes.

This problem, applied to pressure loaded shells of revolution, will be discussed in detail in the remaining portion of this report. A different situation arising from a combination of pressure and centrifugal loads is discussed in Appendix A. This case demonstrates the application of the basic approach to filamentary design of not necessarily isotensoid character and for more complex loading conditions.

III. ISOTENSOID PRESSURE SHELLS OF REVOLUTION

A. Basic Equations

Consider a surface of revolution (r, ρ, z) , as shown in Figure 4, page 42. The coordinates of the vector \bar{X} extending from the origin of a cartesian system (x, y, z) are

$$\bar{X} = \begin{pmatrix} r \cos \rho \\ r \sin \rho \\ z \end{pmatrix} \quad (16)$$

The lines of principal curvature used as surface coordinate lines are the parallel circles $u = z = \text{const}$ and the meridians $v = \rho = \text{const}$.

The differential vector $d\bar{X}$ in terms of the coordinates (z, ρ) , is:

$$d\bar{X} = \frac{\partial \bar{X}}{\partial z} dz + \frac{\partial \bar{X}}{\partial \rho} d\rho = \begin{pmatrix} \frac{dr}{dz} \cos \rho dz - r \sin \rho d\rho \\ \frac{dr}{dz} \sin \rho dz + r \cos \rho d\rho \\ dz \end{pmatrix} \quad (17)$$

The unit vector normal to the surface has the coordinates

$$\bar{e}_n = \begin{pmatrix} \cos \alpha \cos \rho \\ \cos \alpha \sin \rho \\ \sin \alpha \end{pmatrix} \quad (18)$$

where α is the angle between the local surface normal \bar{e}_n and the (x, y) plane.

The second derivatives of \bar{X} , with respect to the principal curvature coordinates, are:

$$\frac{\partial^2 \bar{X}}{\partial z^2} = \begin{pmatrix} \frac{d^2 r}{dz^2} \cos \rho \\ \frac{d^2 r}{dz^2} \sin \rho \\ 0 \end{pmatrix} \quad (19)$$

and

$$\frac{\partial^2 \bar{X}}{\partial \rho^2} = \begin{pmatrix} -r \cos \rho \\ -r \sin \rho \\ 0 \end{pmatrix}$$

From Eq. (5) and (17) the coefficients of the first fundamental form become:

$$\begin{aligned} E_I &= \left(\frac{\partial \bar{X}}{\partial z} \cdot \frac{\partial \bar{X}}{\partial z} \right) = 1 + \left(\frac{dr}{dz} \right)^2 \\ G_I &= \left(\frac{\partial \bar{X}}{\partial \rho} \cdot \frac{\partial \bar{X}}{\partial \rho} \right) = r^2 \end{aligned} \quad (20)$$

Similarly, from Eq. (6), (18), and (19) the coefficients of the second fundamental form become:

$$\begin{aligned} E_{II} &= \left(\frac{\partial^2 \bar{X}}{\partial z^2} \cdot \bar{e}_n \right) = \frac{d^2 r}{dz^2} \cos \alpha \\ G_{II} &= \left(\frac{\partial^2 \bar{X}}{\partial \rho^2} \cdot \bar{e}_n \right) = -r \cos \alpha \end{aligned} \quad (21)$$

From (20) and (21) the principal curvatures of the coordinate lines become:

$$k_{n(v)} = \frac{E_{II}}{E_I} = \frac{\frac{d^2 r}{dz^2}}{\left(1 + \left(\frac{dr}{dz} \right)^2 \right)^{3/2}} = -\frac{1}{\rho_M} \quad (22)$$

$$k_{n(u)} = \frac{G_{II}}{G_I} = -\frac{\cos \alpha}{r} \quad (23)$$

The negative signs appearing in Eq. (22) and (23) are a consequence of the sign conventions used for α and ρ_M , as indicated in Figure 4, page 42.

It is, of course, possible to derive the values of principal curvature by inspection of Figure 4 directly. The analytical development has been given here to demonstrate the application of an approach that may be used for analysis of generalized surfaces.

The normal curvature in direction β becomes, according to Euler's Theorem (7):

$$k_{n\beta} = -\frac{1}{\rho_M} \cos^2 \beta - \frac{\cos \alpha}{r} \sin^2 \beta \quad (24)$$

The direction β of the geodesic filament is obtained by integration of Liouville's Theorem (8) with $k_g(\beta) = 0$. For surfaces of revolution, this integration yields the Theorem of Clairaut (Ref. 4).

$$\sin \beta = \sin \beta_0 \frac{r_0}{r} \quad (25)$$

where $\sin \beta_0$ and r_0 are arbitrary constants of integration.

Let $C = \sin \beta_0$: Filament helix parameter characteristic for the filamentary geometry.

$R = r/r_0$: Non-dimensional radius of shell.

Then, (25) can be written as

$$\sin \beta = \frac{C}{R} \quad (25a)$$

and
$$\cos \beta = \frac{1}{R} \sqrt{R^2 - C^2} \quad (25b)$$

We will now consider a structural shell of revolution consisting of several layers of monotropic membranes, as shown in Figure 5, page 43, subject to a rotationally symmetrical pressure load $p_{(z)}$ that may be variable along the meridian, but is uniform along any parallel circle. Each monotropic membrane is assumed to comprise n_i filaments uniformly spaced along any parallel circle of the shell, each filament of each monotropic membrane forming an angle $\sin \beta_{0_i} = C_i$ with the meridian at the extreme perimeter of radius r_0 , and each filament carrying an equal and uniform axial force T .

The normal load/unit length carried by each filament is

$$F'_{n_i} = p_i \frac{2r_0}{n_i} \cos \beta_i \quad (26)$$

where p_i is the normal pressure carried by each monotropic membrane "i".

The equilibrium condition (14), considering (26) and (24), then becomes

$$-\frac{1}{\rho_M} \cos \beta_i - \frac{\cos \alpha}{r} \frac{\sin^2 \beta_i}{\cos \beta_i} + p_i \frac{2r\pi}{n_i T} = 0 \quad (27)$$

Introducing the "non-dimensional" filament count $N_i = \frac{n_i}{n}$, where n is the total number of filaments traversing a parallel circle, we obtain by substituting (25a) and (25b) into (27)

$$p_i = \frac{nT}{2\pi r_o^2 R} \left\{ \frac{\cos \alpha N_i C_i^2}{R^3} - \frac{r_o}{\rho_M} \frac{N_i \sqrt{R^2 - C_i^2}}{R} \right\} \quad (28)$$

Summing over all monotropic membranes "i", and solving for the non-dimensional meridional curvature yields:

$$\frac{r_o}{\rho_M} = \frac{1}{\sum N_i \sqrt{R^2 - C_i^2}} \left\{ \frac{\cos \alpha}{R} \sum \frac{N_i C_i^2}{\sqrt{R^2 - C_i^2}} - KR^2 \frac{P(z)}{P_o} \right\} \quad (29)$$

where $K = \frac{2\pi p_o r_o^2}{nT}$ is the non-dimensional pressure load parameter which is

characteristic for the curvature properties of the shell.

Eq. (29) describes the meridional curve of the shell of revolution in terms of the intrinsic coordinates ρ_M and α , as a function of the two characteristic parameters C_i and K .

An integral form of Eq. (29) can be derived by considering the equilibrium conditions pertaining to the whole shell, as shown in Figure 5, page 43.

Equilibrium in axial direction requires:

$$(\sum N_i nT \cos \beta_{o_i}) - r_o^2 \pi p_o = (\sum N_i nT \cos \alpha \cos \beta_i) - R^2 r_o^2 \pi P(z)$$

or, solved for $\cos \alpha$:

$$\cos \alpha = \frac{R}{\sum \sqrt{R^2 - C_i^2}} \left\{ (\sum N_i \sqrt{1 - C_i^2}) - \frac{K}{2} (1 - R^2 \frac{P(z)}{P_o}) \right\} \quad (30)$$

Equilibrium in torque around the z-axis for a single filament requires (since the pressure loading can not contribute to a torque):

$$T \sin \beta_i r = T \sin \beta_{o_i} r_o$$

which simply reduces to the Theorem of Clairaut (25) by division through T.

For the complete shell, torsional equilibrium in absence of an externally applied torque requires:

$$\sum N_i C_i = 0 \quad (31)$$

A further condition is imposed for closed pressure vessels of singly connected volume without externally applied axial forces ("Bottles").

For this case, axial equilibrium requires that:

$$\sum N_i \sqrt{1-C_i} = \frac{K}{2} \quad (32)$$

Finally, the problem of defining the filamentary geometry can be solved by integration of the differential geometrical relationship between ρ and α , along a geodesic. By inspection of Figure 4, page 42, we obtain:

$$\rho_M d\alpha \tan \beta = r d\rho$$

or, integrated

$$\rho \alpha - \rho \alpha = 0 = \int_0^{\alpha} \frac{C_i}{R \sqrt{R^2 - C_i^2}} \frac{\rho_M}{r_o} d\bar{\xi} \quad (33)$$

B. Methods of Solution

Eq. (30) represents an integral form of (29) which can be transformed into a first-order non-linear differential equation for $R_{(Z)}$ suitable for numerical integration by substituting

$$\cos \alpha = - \frac{\frac{dR}{dZ}}{\sqrt{1 + \left(\frac{dR}{dZ}\right)^2}}$$

where $Z = \frac{z}{r_0}$ is the non-dimensionalized axial coordinate.

The resulting differential equation can be written in finite difference form for numerical integration by means of a digital computer.

A program has been prepared for an IBM, Type 1620 computer, capable of handling arbitrary inputs for N_i , C_i and K , and computing both intrinsic (ρ, α) and non-dimensionalized cartesian coordinates (R, Z) of the meridional shapes by means of a modified Runge-Kutta method (Ref. 22). Additional output data available from the program are the filament geometry $\rho_{(\alpha)}$ as well as surfaces S and enclosed volumes V of the bodies of revolution generated by rotating the meridional curves (R, Z) around the z -axis.

Analytical solutions of Eq. (30) are possible. These lead to expressions which may be reduced to elliptical integrals. In the general case, however, the resulting expressions are quite involved and time-consuming for evaluation. As a consequence, direct digital integration appears to be a more economical approach for the purpose of obtaining design data. An exception is the case for $C = 0$, discussed in Appendix B. There, the solution can be reduced to simple combinations of elliptical integrals of the first and second kind, which are tabulated, for instance, in Ref. 5.

For the purpose of a graphical solution, Eq. (29) and (30) are suitable in their intrinsic form. Tables of ρ_M and α in function of r/r_0 can be computed for any given set of K , C_i , N_i from Eq. (30) and (29). With slope α and radius of curvature ρ_M known, very accurate meridional shapes can be constructed by means of rule, compass, and protractor.

In addition to the numerical and graphical methods mentioned, the particular case of $C = 0$ (i. e., meridional fiber direction only) allows solution of the isotensoid meridional shape equations by means of a column analog, as shown in Figures 6 and 7, page 44. This analog is described in more detail in Appendix B.

All three methods, digital integration, graphical solution, and column analogy have been used to generate the data shown in Figures 10 through 20, pages 47 through 56.

C. Discussion of Results

For the purpose of an initial evaluation of possible isotensoid pressure vessels, the number of free parameters may be reduced as follows:

(1) The pressure p is assumed to be constant throughout the length of the shell, i. e., $p_{(z)} = p_o = \text{const.}$

(2) The shells are considered to consist of two monotropic membranes satisfying the torque equilibrium equation (31):

$$\text{where } N_1 = N_2 = .5$$

$$\text{and } C_1 = -C_2 = C$$

With these assumptions, the intrinsic equations (29) and (30) reduce to

$$\frac{r_o}{\rho_M} = \frac{1}{\sqrt{R^2 - C^2}} \left\{ \frac{\cos \alpha}{R} \frac{C^2}{\sqrt{R^2 - C^2}} - KR^2 \right\} \quad (29b)$$

and, in integral form:

$$\cos \alpha = \frac{R}{\sqrt{R^2 - C^2}} \left\{ \sqrt{1 - C^2} - \frac{K}{2} (1 - R^2) \right\} \quad (30b)$$

where C and K are the defining parameters of the isotensoid pressure shell.

Inspection of Eq. (29b) and (30b) shows that no real solution for either ρ or α exist if $R < C$. Thus, the minimum distance from the axis of rotation which a geodesic filament can have is given by its helix angle defined by C . An important design implication that may be derived from this is that there will always be a polar opening for any geodesically helix wound ($C \neq 0$) pressure vessel. The size of the polar opening R_{\min} can be computed from Eq. (30b) by letting

$$\cos \alpha = \pm 1$$

Excluding the trivial solution $R = 1$, we obtain a relation between K , C and R_{\min} :

$$\frac{K}{2} (1 - R_{\min}^2) = \mp \left\{ \frac{\sqrt{R_{\min}^2 - C^2}}{R_{\min}} - \sqrt{1 - C^2} \right\} \quad (34)$$

This equation is useful if R_{\min} is given as a design parameter, and a compatible pair C and K need to be determined for the design of the pressure vessel.

The solutions that may be obtained for the meridional shapes $R_{(z)}$ by solution of the intrinsic equations (29b) and (30b) can be classified according to their general character for a range of parameter K .

For the purpose of this discussion, only the range of $K \geq 0$ will be considered. Negative K -values yield similar shapes (corresponding to either negative pressure or compressive fiber force) and yield no new general insight into the problem even though they may be important for particular design objectives. The various shapes for positive K -values are discussed below and are shown in schematic form in Figures 8 and 9, pages 45 and 46:

(1) Hyperboloid (Figure 8a)

Here the extreme perimeter r_o is a minimum. For all positive z , $\cos \alpha$ is always negative and ρ_M is always positive. This requires $K = 0$ and results in the filaments being straight lines rotating around the z -axis, forming a hyperboloid of revolution. This is a surface of zero curvature, corresponding to zero internal pressure p .

(2) Cylinder (Figure 8b)

For a cylinder $R \equiv 1$, $\cos \alpha \equiv 0$ and $\rho_M = \infty$. These conditions are satisfied if

$$K = \frac{C^2}{\sqrt{1 - C^2}}$$

(3) Corrugated Tube (Figure 8c)

A corrugated tube will exhibit a point of inflection where $\rho_M = \pm \infty$ at a value of $R > C$. α will always be smaller than $\pm \frac{\pi}{2}$.

This requires that

$$0 < K < \frac{2}{\sqrt{1 - C^2}}$$

If $K < \frac{C^2}{\sqrt{1-C^2}}$, then the corrugations are located outside the cylinder $R = 1$ and r_o is a minimum; if $K > \frac{C^2}{\sqrt{1-C^2}}$, then the corrugations are inside the cylinder $R = 1$, and r_o is a maximum, as indicated in Figure 8c.

For those corrugated tubes ("bottles") which satisfy the axial equilibrium equation (32), the following relations hold:

The minimum radius R_{\min} is related to the fiber helix parameter C by

$$\sqrt{1-C^2} = \frac{\sqrt{R_{\min}^2 - C^2}}{R_{\min}^3}$$

The slope α of the meridian is given by

$$\cos \alpha = R^3 \sqrt{\frac{1-C^2}{R^2 - C^2}}$$

The radius at the inflection point of the meridian is

$$R_{(\rho=\infty)} = \sqrt{3/2} C$$

The slope at the inflection point is given by

$$\cos \alpha_{(\rho=\infty)} = \frac{3}{2} \sqrt{3} C^2 \sqrt{1-C^2}$$

(4) Cusp (Figure 8d)

For the case of a cusp, the angle α becomes indefinite and ρ_M becomes 0 at $R = C$. This condition is satisfied if

$$K = \frac{2}{\sqrt{1-C^2}}$$

The cusp shape constitutes the transition between the corrugated tube and the progressive loop.

(5) Loop (Figure 9)

Looped curves which are of particular interest for the generation of toroidal pressure vessels, are generated if ρ_M is negative for all values of R . This requires

$$K > \frac{2}{\sqrt{1-C^2}}$$

Three distinct types of loops are generated as K increases:

- (a) A progressive, periodic loop (Figure 9a), page 46.
- (b) A closed loop forming the transition between progressive and regressive, periodic loops (Figure 9b), page 46.
- (c) A regressive, periodic loop (Figure 9c), page 46.

The radius R_H at which the meridional curve is horizontal (i. e., the location of maximum thickness of the toroid generated by rotation of the loop) is

$$R_{(\alpha = \pi/2)} = \sqrt{1 - \frac{2}{K} \sqrt{1 - C^2}}$$

A summary of the domains in the positive K-C plane corresponding to the various types of solutions is shown in Figure 10, page 47. Also shown in Figure 10 are the curves $R_{\min} = \text{const}$, and the C-K values resulting in "bottles" according to Eq. (32).

A number of cases for various parameter combinations have been worked out by digital integration of Eq. (30) and (33) complemented by graphical and column analog studies. Primary attention was given to the looped type of solutions which are of interest in the design of toroidal pressure vessels.

Figures 11 through 14, pages 48 through 51, show the meridional shapes for 1/2 period ($0 \leq \alpha \leq \pi$) of double helix wound shells according to Eq. (29b) and (30b) for $K \geq \frac{2}{\sqrt{1 - C^2}}$ and for C-values of 0, .25, .5, and .75, respectively.

Figures 15 through 17, pages 52 through 54, show solutions for the case of looped meridians for shells consisting of three layers $C_1 = 0$, $C_2 = .5$, $C_3 = -.5$ with variable ratios of N_1/N_2 and with $N_2 = N_3$.

Figure 18, page 55, shows a case with 6 layers, representing the case of a corrugated tube, together with the elementary geometry of the various layers.

In the cases of multiple C-values, shown in Figures 15 through 18, return points occur at $R = C_i$, where the corresponding monotropic membrane folds back into itself, reversing the helix angle and thus forming $C_{i+1} = -C_i$.

Figure 19, page 56, shows an example of an unsymmetrical loop resulting

from linearly variable pressure simulating the situation of a pressure vessel subject to hydrostatic pressure gradients such as may be encountered in a liquid container during the boost phase of a rocket.

Figure 20, page 56, shows a realization of the particular case for a closed loop indicating the general shape and the disposition of the winding pattern.

IV. MORPHOLOGY OF CLOSED PRESSURE VESSELS

The range of possible isotensoid pressure shells of revolution with meridional shapes as shown in Figures 11 through 20, is limited by the restriction of the parameter ranges and combinations that have been considered. Nevertheless, five basic types of possible closed pressure vessel designs are identifiable from a review of the presented material. A brief discussion of their general characteristics follows:

A. Containers With Simply Connected Volume

1. Type I: (Figure 21, page 57). Closed shells containing a monotropic membrane with meridional fiber direction ($C = 0$) crossing the z-axis.

In the special case where the "bottle" relationship of K and C_i , given in Eq. (32) is satisfied, the meridian crosses the z-axis at right angles, and simple closed "bottles" result. Where the parameters K and C_i do not satisfy Eq. (32), additional elements in the form of an axial compression column or tension rod located in the z-axis are necessary for equilibrium. A discussion of such shapes has been given in Ref. 8.

Shells containing monotropic membranes with $C = 0$ are, from a practical point of view, not realizable in pure form, since all fibers of the $C = 0$ layers cross the z-axis at the same location, resulting in a "pole" singularity, and generating an impractical local buildup of material in the winding pattern at the pole. This form of pressure vessel has been approached by employing very small helix angles β_0 (or small C -values). Such structures have been made in the form of the "Bermuda bottles" ($C \sim 0$, $K \sim 2$), and as enclosures of "end-over-end" wound cylinders produced by several manufacturers of filament-wound pressure vessels.

Other possibilities in reducing the polar problem rest in the use of wide bands for the $C = 0$ layers. An example is shown in Figures 37 and 38, page 66.

2. Type II: (Figure 22, page 58): Closed bottles of singly connected volume incorporating a secondary closure structure for the polar openings.

This type of pressure vessel needs to satisfy Eq. (32) for axial balance unless axial tension or compression members supporting unbalanced endclosure forces are added to the design. As seen from Figure 10, all "bottles" fall in the realm of monotropic membranes in the form of corrugated tubes. These corrugated tubes can be modified to include a cylindrical portion of $R = 1$ between two converging portions by application of a circumferential winding pattern ($C = 1$). Such "bottles" represent the ideal design for the familiar type of filament-wound cylindrical pressure vessels and rocket motor cases with "ovaloid endclosures" (Ref. 9).

A section of a "corrugated tube" will have two polar openings with a minimum radius of $R_{\min} \geq C_{i\min}$. If a polar opening $R > C_{i\min}$ is required (for instance, for nozzle attachments, etc.) then a circumferential retaining hoop ($C = 1$) must be inserted into the winding pattern to obtain balance of an isotensoid structure (Ref. 19) requiring a special winding arrangement. In either case, a secondary closure structure, normally consisting of a flanged ring or disk insert, must be provided.

A discussion of the detail design problems for the flange attachments is beyond the scope of this report. Suffice it to note that the proper flange shapes may be derived from the basic equations for isotensoid shells by introducing the contact pressure between flange and filamentary shell into the equations.

As in the case for Type I, excessive buildup of filaments at the polar opening (i. e. , at the "turn around" point of the winding pattern) may result. This problem can be reduced by use of a tension hoop (Ref. 19), as discussed above, which prevents the filaments from piling up at the turn around. Other solutions that have found practical application consist of using filaments of finite width (ribbon-winding) or by small variations of the filament helix angle around a mean value (wobble-winding), which tends to spread the buildup over a finite domain of the interface area.

B. Container with Doubly Connected Volume

1. Type III: (Figure 23, page 59): Closed toroids (doubly connected volumes) generated from progressive loops.

Progressive loops, as shown in Figure 9a, may be used to generate close toroidal pressure vessels in two ways:

- a. A compression-resistant hub structure may be used to provide internal closure of a loop extending between two minimum perimeters R_{\min} of the meridional curve. The filaments, in this case, may either be continuous around the torus meridian, or they may return around retaining hoops located at the hub rims in the fashion of an automobile tire, similar to the one shown for Type II in Figure 22, page 58.
- b. A compression-resistant hoop may be introduced in the outward cusp of a single loop, providing the necessary circumferential balance forces.

In either case, compression-resistant structural components are required to close the pressure vessel. As a result, the elastic deformation of the shell due to pressurization cannot yield a geo-

metrically similar shape which insures uniform strain in each filament. Mismatched deformations in the various components of the shell will normally take place, and deviations from ideal isotensoid conditions will be encountered in most cases.

2. Type IV: (Figure 24, page 60): Closed toroids from closed loops.

Closed loops, as shown in Figure 9b, form an ideal basis for the design of isotensoid toroidal pressure vessels, unless large access holes or valve openings are required by the particular design application.

3. Type V: (Figure 24): Closed toroids generated from regressive loops.

Regressive loops, as shown in Figure 9c, may be used to form closed toroidal pressure vessels in a similar fashion, as discussed for Type III:

- a. Tension-resistant outer equatorial bands of finite width ($C = 1$) may be used to provide external closure of a loop extending between two maximum perimeters r_o of the meridional curve.
- b. A tension-resistant hoop may be introduced in the inward cusp of a single loop, providing the necessary circumferential balance forces.
- c. Of practical importance is the case where both outer bands and an inner hoop are used for a complete torus structure. The free choice of width and/or spacing in the outer bands allows greater freedom in obtaining particular design characteristics. Further, the use of several bands allows construction of stable toroidal pressure vessel configurations with only meridional ($C = 0$) and perimetral ($C = 1$) windings.

As opposed to the Type III, Type V employs tension-resistant material only, thus, the conditions of uniform extension throughout the structure may be satisfied by proper dimensioning of the bands and hoops.

A review of the various isotenoid pressure vessels forming shells of revolution indicates that in practice only the toroidal Types IV and V can be made as completely closed containers and requiring only tension-resistant filamentary material.

These types promise to be of interest in two aspects:

1. Where foldable, pneumatically stabilized structures are required, filamentary materials made from strong fibers imbedded in an elastic matrix may be used. The absence of any rigid, compression-resistant members favors the Types IV and V for such application.
2. Secondly, the monolithic structure of Types IV and V, and absence of additional weights due to enclosures, such as required for Type II, promises a high structural efficiency for the toroidal shapes.

Toroidal isotenoid pressure vessels have been selected for experimental verification of the theoretically derived data in Part Two - "Experimental Investigations" - of this report.

V. CONCLUDING REMARKS

Several areas of investigation, pertinent to the practical design implementations for isotensoid pressure vessels, have been covered only briefly during this investigation. The following paragraphs are intended to indicate directions for further studies.

A. Structural Weights, Enclosed Volumes, and Surface Areas of Isotensoid Pressure Vessels

The theoretical structural weight of an isotensoid pressure vessel has been derived from energy considerations in Refs. 8 and 10:

$$W_s = 3 \frac{V_p (SF)}{l}$$

where V: Enclosed volume of pressure vessel.

p: Working pressure.

(SF): Safety factor.

l: Specific strength of unidirectional material.

From this equation the surprising conclusion follows that the theoretical weight of a pressure vessel made from a given material to enclose a given volume under a given pressure is independent of its general shape, provided it satisfies the conditions of isotensoid design.

As discussed in Ref. 10, the actual weight exceeds the theoretical for several reasons, such as premature failure due to design deficiencies, and additional weights from "bottle" enclosures, leakage barriers, attachments, etc.

While the toroidal isotensoid shapes of Type IV and V may be expected to be superior to others with respect to design efficiency and absence of weights associated with auxiliary structural members, etc., they will normally exhibit relatively large surface areas for a given enclosed volume, resulting in low structural wall thickness. This is advantageous from the point of view of fold-

bility for expandable structures. It also results, however, in a relatively large weight contribution of leakage barriers required for pressure tightness.

The non-dimensionalized volume-to-surface area ratio V/Sr_o has been worked out for toroidal pressure vessels of Type V-b for a range of C and K-values. The results are plotted in Figure 26, page 62. From this plot it appears that the V/Sr_o -value is, for practical purposes, independent of C and a function of K only for the particular type of toroidal isotensoid pressure vessel considered.

B. Periodicity of Winding Patterns

In the practical realizations of winding patterns, a uniform distribution of the fibers over the mandrel is desired. Ideally, this may be accomplished by selecting a fiber geometry where the filament is displaced by a unit filament spacing after each complete revolution $\phi = 2\pi$ of the mandrel. The same effect is produced if the central angle of mandrel revolution for each filament revolution is a rational fraction of $2\pi + \delta$, where δ is the central angle of the desired filament spacing. In this case, a multiple number of mandrel revolutions is necessary until the filament becomes again adjacent to itself. An example of this type is shown in the filamentary geometry of Figure 20 where $\phi(\alpha = 2\pi)$ has been selected as $\frac{4\pi}{9}$, thus, two mandrel revolutions and nine filament revolutions will constitute a full period in the filamentary pattern.

The relation of the central angle for a complete filament revolution $\alpha = 2\pi$ can be obtained by integration of Eq. (33). Data have been worked out over a range of C-values for isotensoid pressure vessels of Type IV. Results in the form of $\phi(\alpha = 2\pi)$ vs C are plotted in Figure 27, page 63.

C. Instability Phenomena in Toroidal Pressure Vessels

Instability phenomena have been observed in toroidal pressure vessels and reported, for instance, in Ref. 10. Such instabilities will be expected particularly in those cases which are of structurally underdeterminate nature, i. e., in shells containing two or less fiber directions in certain domains of the structure. The instability mechanisms are very similar to those observed in magnetic

bottles designed to confine plasma at high pressure, where the magnetic lines of force take the place of the filamentary texture (see, for instance, Ref. 11).

Other types are those found in soap bubbles (Ref. 12) or of the nature of hydrostatic instability for straight cylindrical tube made from isotropic material (Ref. 13).

Instability phenomena have also been observed during the experimental program discussed in Part Two of this report. A number of test models have been designed to elucidate the various possible shapes that are obtained, some of them exhibiting striking geometrical symmetry and beauty. Figures 28 through 31, page 64, shows a number of those shapes, obtained from toroidal pressure vessels of Type V.

While, for the purpose of pressure-containing, the instability phenomena are detrimental, it is well conceivable that these may be purposely used for control of geometry where such control is a functional requirement.

D. Non-Monotropic Filamentary Textures

The study presented here has been essentially confined to filamentary textures that may be produced by filament winding processes, and may be idealized as arrays of monotropic membranes.

There are obviously many other possible arrangements, differing in their degree of orientation and in their topological character. A possible approach to the discussion of these textures may originate from a study of their production processes. Such processes, familiar from the textile and wire industry, may involve:

Weaving	Braiding
Meshing	Crocheting
Netting	Mailling
Looping	Matting
Knitting	etc.

The filament winding process is apt to yield the best possible directional strength and fiber density for a structure. Other processes, however, may have

structural advantages, particularly where foldability is required.

Figures 32 and 33, page 65, show a toroidal pressure vessel made from a knitted filamentary texture, in inflated and deflated (folded) condition. The advantage of the knitted texture is its ability to absorb large membrane distortions in its own plane; thus, the possible folding mechanisms and folding geometries are not restricted to those of isometric nature (Ref. 20).

Figure 34, page 65, shows a combination of a knitted structure combined with filament-wound reinforcing bands, producing a "corrugated toroid" structure.

Figure 35, page 66, shows a tubular structure made from knitted tungsten wire, indicative of the possibilities in forming high-temperature-resistant variable geometry structures useful, for instance, as aerodynamic re-entry control devices.

A somewhat different topology of meshed wire indicative of possible variations for filamentary structures is shown in Figure 36, page 66.

E. Isotensoid Pressure-Stabilized Structures Subjected to Concentrated Loads

Practical applications of load carrying, pressure-stabilized structures frequently involve concentrated loadings:

- (1) Problems associated with one type of concentrated loading arising from the flange interface pressure originating from endclosure inserts and attachments in pressure containers of Type II have been briefly mentioned in paragraph IV.
- (2) Another case of concentrated loading is represented, for instance, by the toroidal pressure vessel of Type V that can be generated by rotation of the unsymmetrical loop shown in Figure 19. The resulting toroidal pressure vessel will be designed for a hydrostatic gradient load resulting from a heavy liquid. The reaction to the liquid weight results in an axial load component. This component may be provided by a concentrated loading acting upon the tension hoop placed into the inside cusp of the toroid formed from the loop.

The same force also provides equilibrium for the unsymmetrically disposed, isotensoid filament forces acting on the hoop.

- (3) A third case of a concentrated side load applied to a pressure vessel of modified Type I is shown in Figure 37, page 66. Figure 38, page 66, shows the same pressure vessel in a folded, de-pressurized state, demonstrating the bending flexibility of the materials used in the shell construction.

Of interest in each of the three cases of concentrated load application discussed above is the fact that the isotensoid character of the structure is retained despite the concentrated load application; thus, an optimum-load-bearing design for pressure-stabilized structures may be evolved.

REFERENCES

1. Struick, D. J. : Differential Geometry, Addison Wesley Press, 1950.
2. Haack, Wolfgang: Elementare Differentialgeometrie, Birkhauser Verlag Basel, 1955.
3. Coxeter, H. S. M. : Introduction to Geometry, John Wiley, Inc. , 1961.
4. Clairaut, A. C. : Mem. Acad. Paris, 1733.
5. Jahnke, E. , Emde, F. : Tables of Function, Dover Publications, 1945.
6. McLachlen, R. : Ordinary, Non-Linear Differential Equations, Oxford Univ. Press, 1956.
7. Southwell, R. V. : Theory of Elasticity, Oxford Univ. Press, 1946.
8. Hoffman, G. A. : The Effect of Filamentary Materials on Pressure Vessel Design, International Astronautical Congress, Stockholm, Sweden, August 1960.
9. Young, R. E. : History and Potential of Filament Winding, 13th Annual Tech. & Management Conference Reinforced Plastics Division, Society of the Plastics Industry, Chicago, Illinois, February 4, 1958.
10. Schuerch, H. : Space Structure Design with Composite Materials, Astro Research Corporation, ARS Preprint 1096-60, April 1960.
11. Koller, A. : Confining A Plasma by a Magnetic Field, ASTIA Document No. AD 254 017, April 1961.
12. Boys, C. V. : Soap Bubbles, Their Colours and the Forces Which Mould Them, Dover Publications, 1959.
13. Mills, B. D. Jr. : The Fluid Column, American Journal of Physics, April 1960.

REFERENCES (Continued)

14. Schuerch, H. U., Kyser, A. C.: Isotensoid Torus Design - Final Report, ASTRO RESEARCH CORPORATION, Contract NAS1-889, February 16, 1961.
15. Riley, M. W., Lieb, J. H., et al: Filament Wound Reinforced Plastics: State of the Art, Reprint from Materials in Design Engineering, August 1960.
16. Filament Winding Conference, Society of Aerospace Material & Process Engineers, March 28-30, 1961.
17. Hedgepeth, J. M.: Stress Concentrations in Filamentary Structures, NASA TN D-882, May 1961.
18. Brenner, S. S.: Growth and Properties of Whiskers, Science, Volume 128, September 12, 1958.
19. U. S. Patent Application: Isotensoid Structures, Serial No. 859,473. Assigned to ASTRO RESEARCH CORPORATION.
20. Schuerch, H. U., Schindler, G. M.: A Contribution to the Theory of Folding Deformations in Expandable Structures with a Particular Application to Toroidal Shells, ASTRO RESEARCH CORPORATION, Contract NASr-8, July 20, 1961.
21. Schuerch, H. U.: Preliminary Study of Application of Advanced Structural Materials to Space Vehicles and Boost Systems, TEMPO, RM 59TMP-9, January 31, 1959.
22. Scarborough, J. B.: Numerical Mathematical Analysis, John Hopkins Press, 1950.

APPENDIX A

MONOTROPIC SHELLS SUBJECT TO CENTRIFUGAL LOADING AND PRESSURE

Consider a monotropic membrane in the form of a shell of revolution similar to the one shown in Figure 5.

In addition to the normal load/unit length of filament due to a uniform internal pressure we will now also consider a radial load vector \bar{F}'_{ω} caused by a rotation of the shell around the z-axis with an angular velocity ω .

$$\bar{F}'_{\omega} = m' r \omega^2 \begin{pmatrix} \cos \beta \\ \sin \beta \\ 0 \end{pmatrix} \quad (1A)$$

where m' is the mass associated with a unit length of the filament.

The tangential component of this load vector is obtained by scalar multiplication with the unit tangent vector \bar{e}_t :

$$F'_t = (\bar{F}'_{\omega} \cdot \bar{e}_t) = m' r \omega^2 \cos \beta \sin \alpha \quad (2A)$$

The first equilibrium equation (13) becomes

$$\frac{dT}{ds} + m' r \omega^2 \cos \beta \sin \alpha = 0$$

and, since $dr = -ds \cos \beta \sin \alpha$:

$$dT = m' r \omega^2 dr$$

which integrates to

$$T - T_0 = m \omega^2 \frac{1}{2} (r^2 - r_0^2)$$

or

$$T/T_0 = 1 - \frac{\Omega}{2} (1 - R^2) \quad (3A)$$

where T_0 is the fiber force at r_0 and $\Omega = \frac{m' \omega^2 r_0^2}{T_0}$ is the non-dimensionalized centrifugal load parameter. Thus, the fiber force is non-uniform and an "isotenoid" design would require a tapering cross-section of filaments designed to keep the filament stress and strain uniform.

The equilibrium conditions for the shell of revolution in axial direction and in torque remain unaffected by the centrifugal force field. Thus, Eq. (25a) becomes, for a single monotropic membrane

$$T \sin \beta R = T_0 C \quad (4A)$$

Since in general T/T_0 will differ from unity, the fiber paths are obviously no longer geodesics. This may be verified by comparing (4A) with Clairaut's Theorem given in the form of Eq. (25a).

The axial equilibrium equation (30) becomes for a single monotropic membrane:

$$n T_0 \cos \beta_0 - r_0^2 \pi p = n T \cos \alpha \cos \beta - R^2 r_0^2 \pi p$$

or

$$\sqrt{1 - C^2} - \frac{K}{2} (1 - R^2) = \cos \alpha \sqrt{\left(\frac{T}{T_0}\right)^2 - \frac{C^2}{R^2}} \quad (5A)$$

where K is defined by

$$K = \frac{2 \pi r_0^2 p}{n T_0}$$

Solving (5A) for $\cos \alpha$ and substituting (3A) for T/T_0 yields the intrinsic equation for the meridional shape of a monotropic membrane subject to both a uniform internal pressure and a distributed centrifugal load associated with a rotation around the z -axis and a uniform mass distribution per unit length of the filaments:

$$\cos \alpha = \frac{\sqrt{1 - C^2} - \frac{K}{2} (1 - R^2)}{\sqrt{\left[1 - \frac{\Omega}{2} (1 - R^2)\right]^2 - \frac{C^2}{R^2}}} \quad (6A)$$

Thus, the equilibrium shape is delivered by three characteristic parameters:

- (1) The parameter defining the fiber geometry: C .
- (2) The parameter defining the pressure loading: K .
- (3) The parameter defining the centrifugal loading: Ω .

APPENDIX B

MERIDIONALLY WOUND ISOTENSOID PRESSURE VESSELS

For the particular case of $C \equiv 0$ (i. e., meridional fiber direction only) and for $p = p_0 = \text{const}$, Eq. (29) and (30) reduce to

$$\frac{r_0}{\rho_M} = -KR \quad (1B)$$

$$\cos \alpha = 1 - \frac{K}{2} (1 - R^2) \quad (2B)$$

It can be shown (Ref. 14) that the shape of a buckled slender column with large deformations, subject to eccentric loading, as shown in Figure 6, satisfies an equation of the form (1B) as follows:

Let EI = bending stiffness of column
- P = compressive load

Then the equilibrium condition for the buckled column becomes

$$-Pr = \frac{EI}{\rho} \quad \text{or}$$

$$\frac{1}{\rho} = -\frac{P}{EI} r \quad (3B)$$

which can be transformed into Eq. (1B) by setting

$$K = \frac{P}{EI}$$

Analytical solutions to this classical problem ("The Elastica") lead to tabulated elliptical integrals of the first and second kind (Ref. 5), and have been worked out in detail by several authors (see, for instance, Ref. 6 and 7). The derivations will not be reproduced here, but only the principal results will be summarized.

The lengths s of the column (or meridional lengths of the isotensoid pressure vessel) is related to the parameter $K = \frac{P}{EI}$

by

$$s = 2 \sqrt{K} \mathcal{F}(k, \pi/2) \quad (4B)$$

where:

- \mathcal{F} : Elliptical integral of the first kind
 k : Characteristic argument of elliptical integral.

The maximum deflection r_o of the column (or perimetral radius r_o of the isotensoid pressure vessel) is:

$$r_o = 2k \sqrt{K} = \frac{ks}{\mathcal{F}(k, \pi/2)} \quad (5B)$$

The distance h between ends of the buckled column (or between the poles of the isotensoid membrane) is

$$h = 2 \sqrt{K} [2 \mathcal{E}(k, \pi/2) - \mathcal{F}(k, \pi/2)] \quad (6B)$$

where:

- \mathcal{E} : Elliptical integral of the second kind.

The "column analogy" for the meridional isotensoid uniform pressure vessel has proven useful in gaining insight into the types of solutions that can be expected. A workable analog device suitable for general study has been constructed from a thin piano wire, loaded by axial forces over adjustable bars, as shown in Figure 7.

Several solutions for the case $C = 0$ are shown in Figure 11. Their general character shows a peculiarity, which has been discussed in Ref. 8:

The cusp case ($K = 2$) represents a closed ovaloid (Bermuda bottle). Alternating loops crossing the z -axis between each maximum occur between $K = 2$ and

$K = 4$. These loops are progressive for $2 < K < 3.32$ and regressive for $3.32 < K < 4$. The transition case of $K = 3.32$ represents a figure resembling a lemniscate from which a degenerated closed toroid of vanishing inner perimeter can be formed by rotation around the z -axis.

The case $K = 4$ represents an aperiodic loop with both branches asymptotic to the z -axis.

For $K > 4$, regular, regressive periodic loops such as shown in Figure 9c occur.

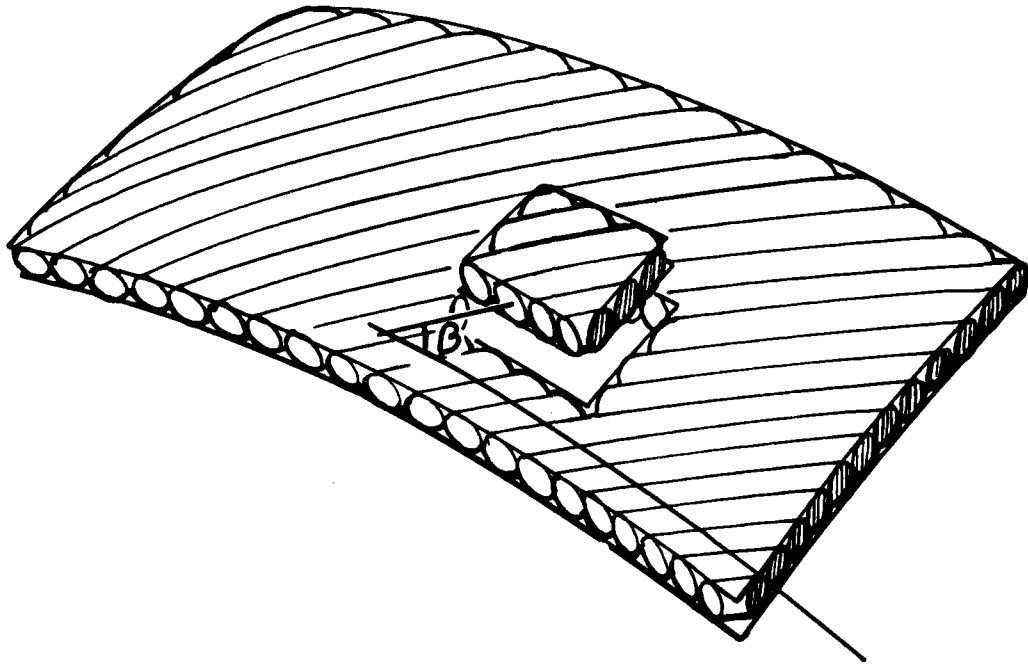
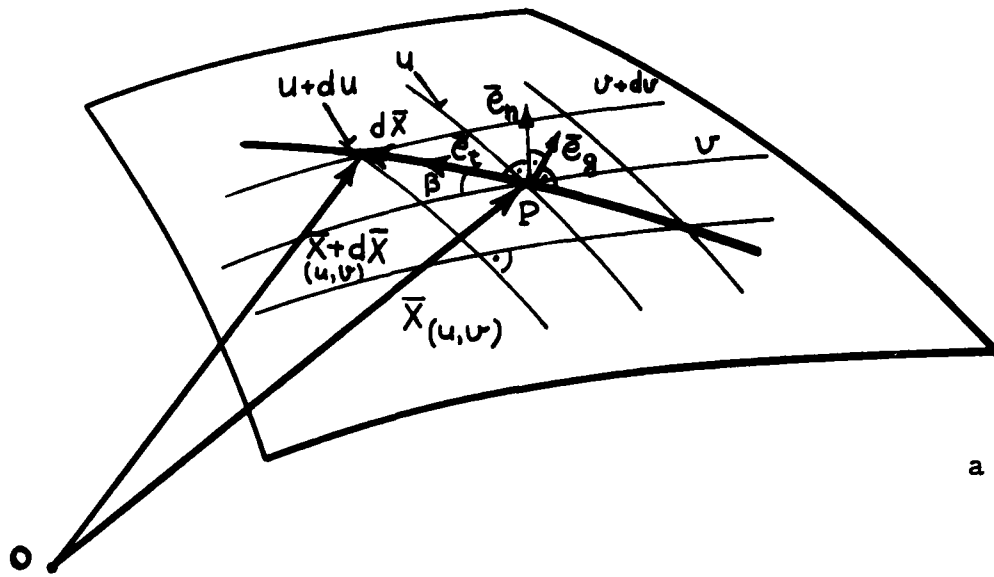
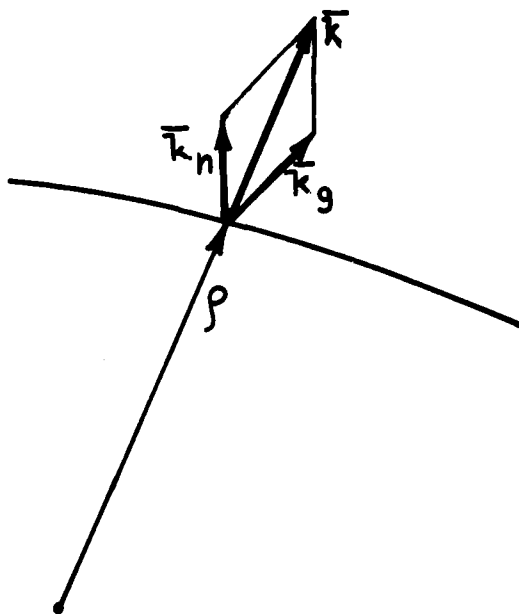


FIGURE 1-Monotropic Membrane



a



b

FIGURE 2-Coordinate Systems and Fiber Geometry For Generalized Surface

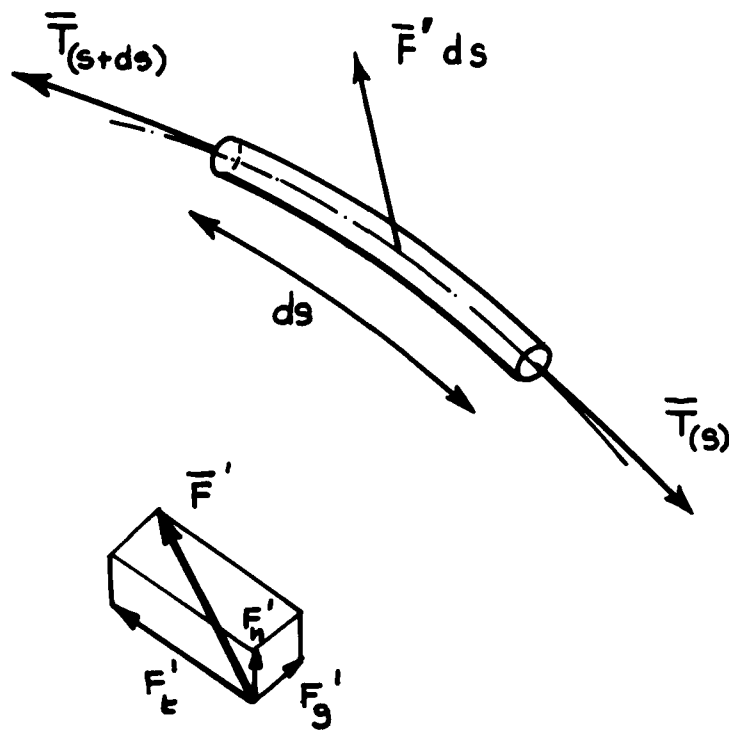


FIGURE 3- Forces On Filament Element

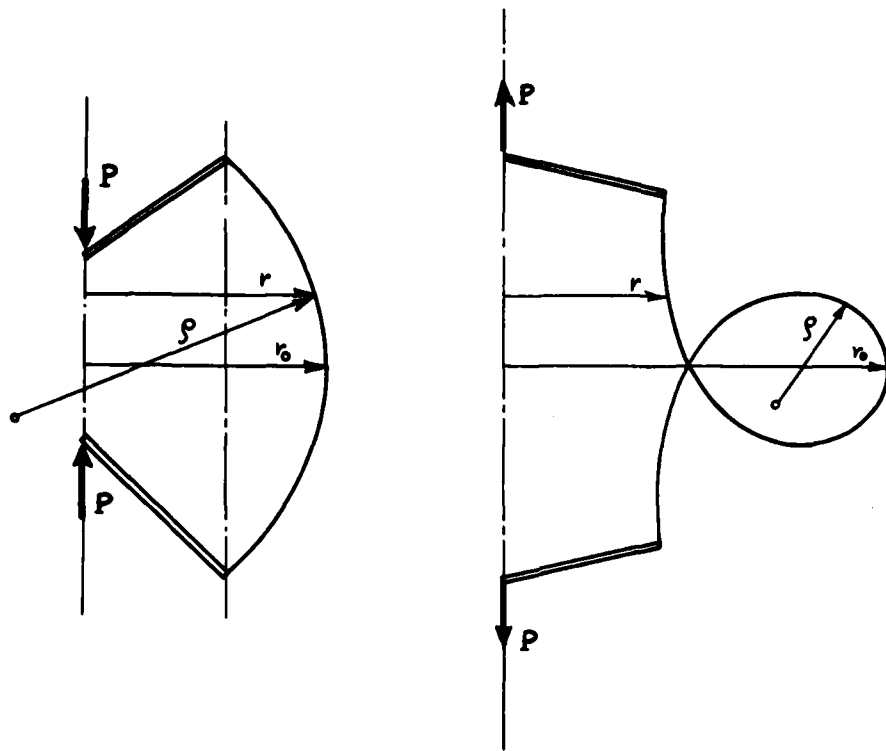


FIGURE 6-Column Analogy

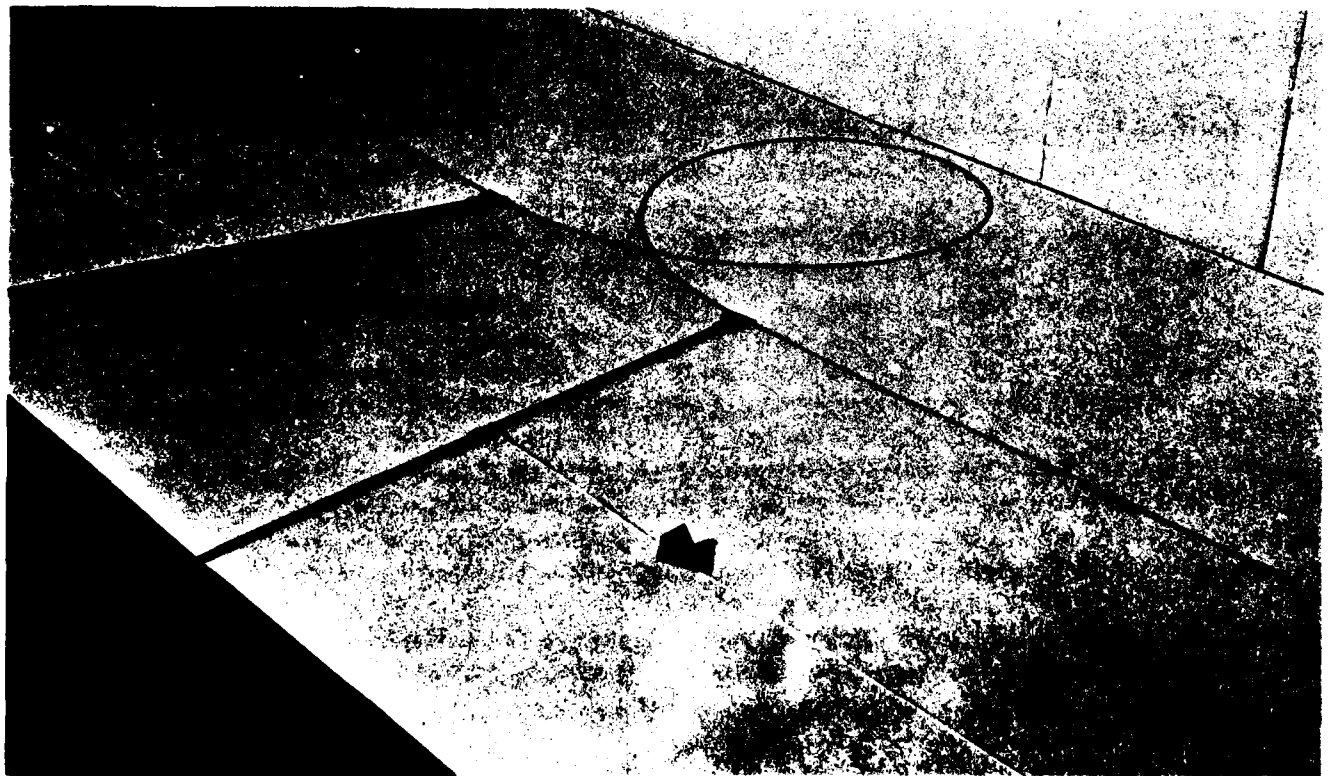


FIGURE 7-Column Analog Apparatus

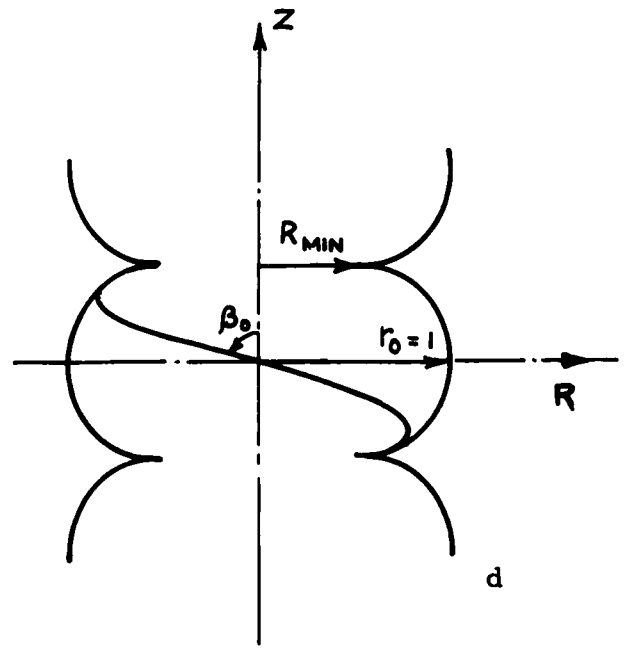
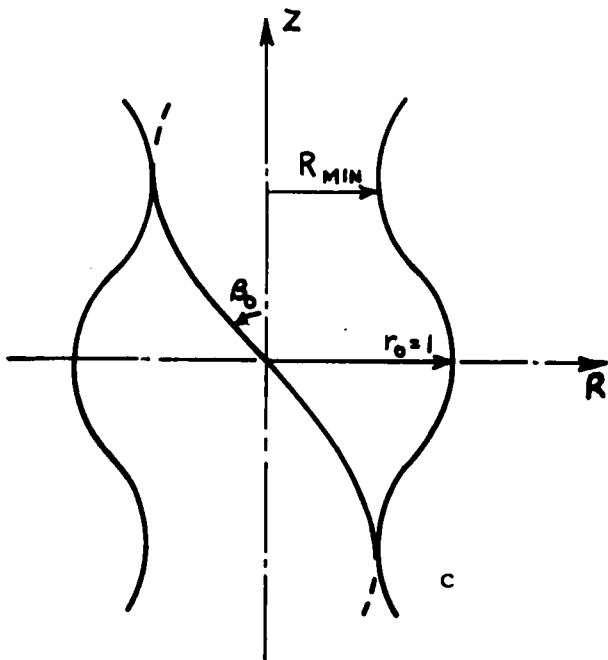
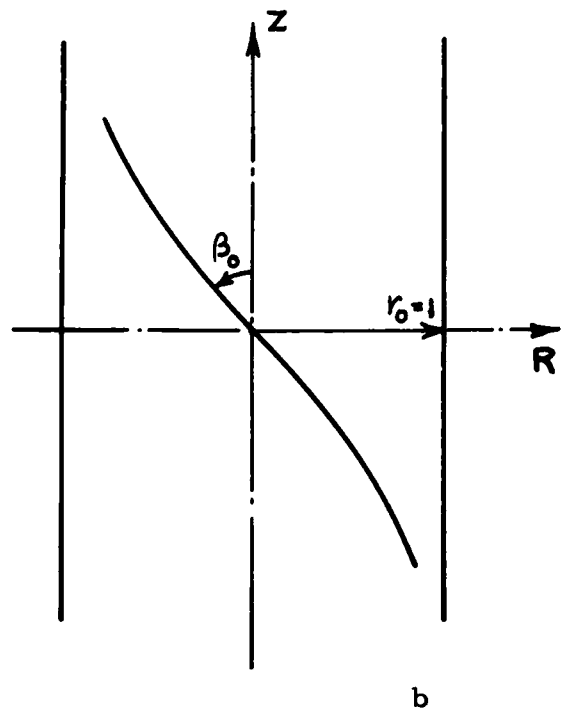
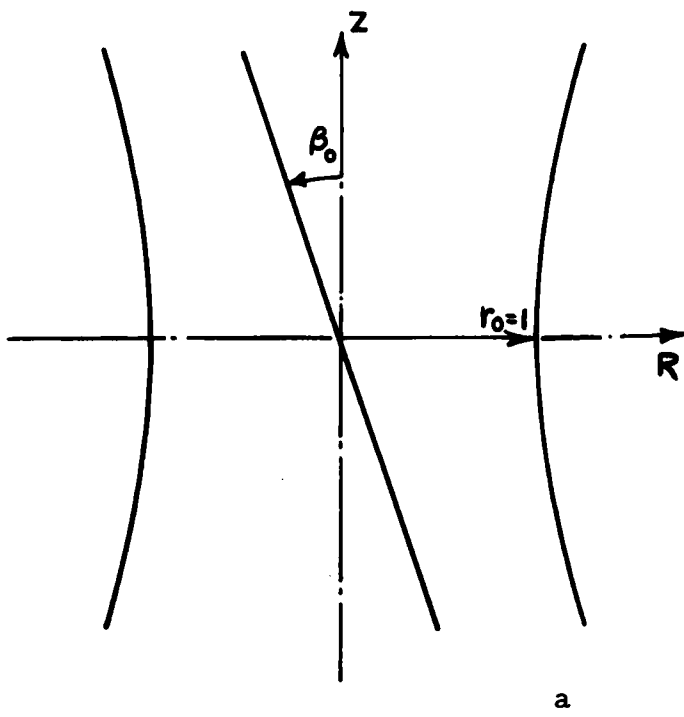


FIGURE 8-Isotensoid Meridional Shapes

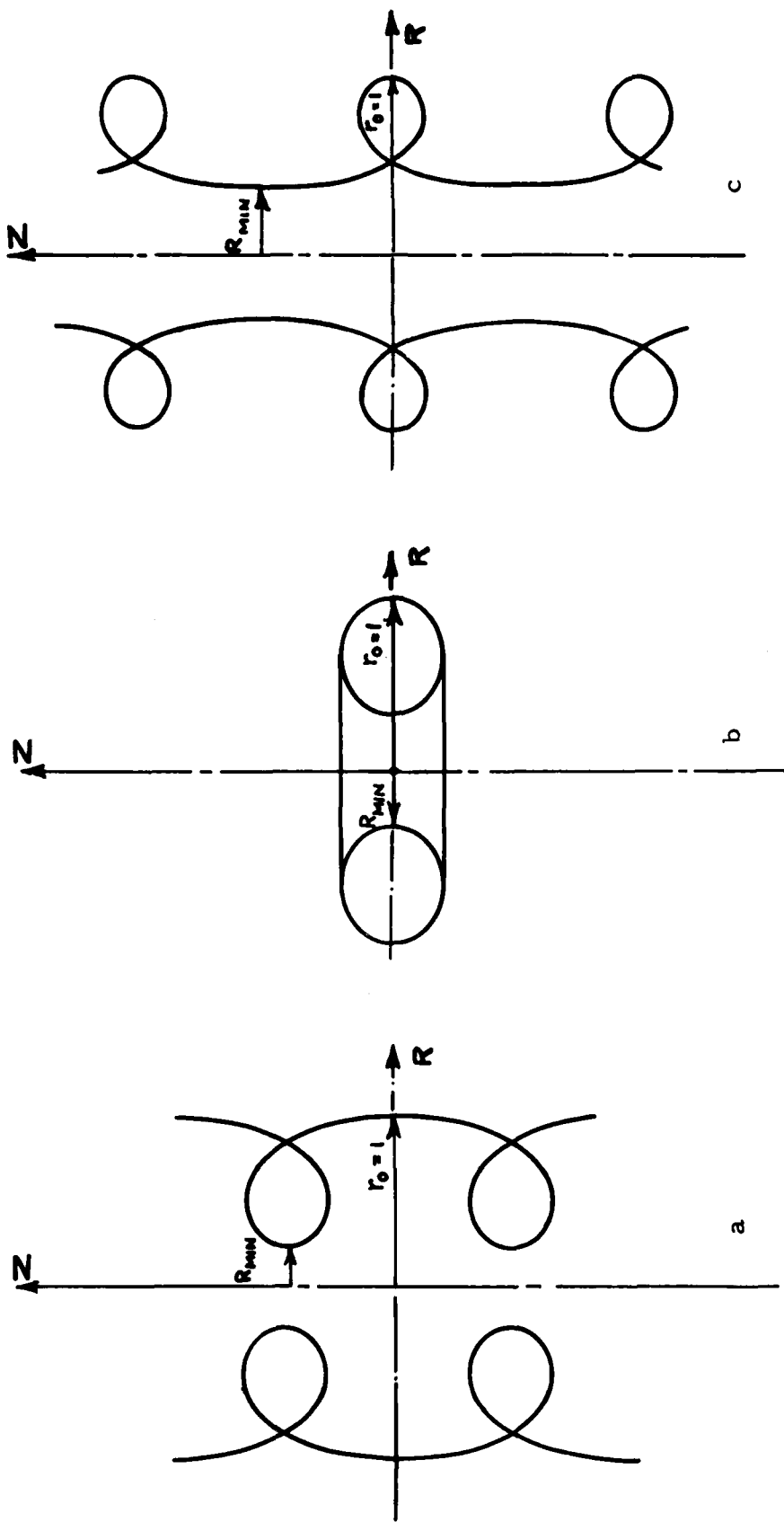


FIGURE 9 - Isotenoid Meridional Shapes

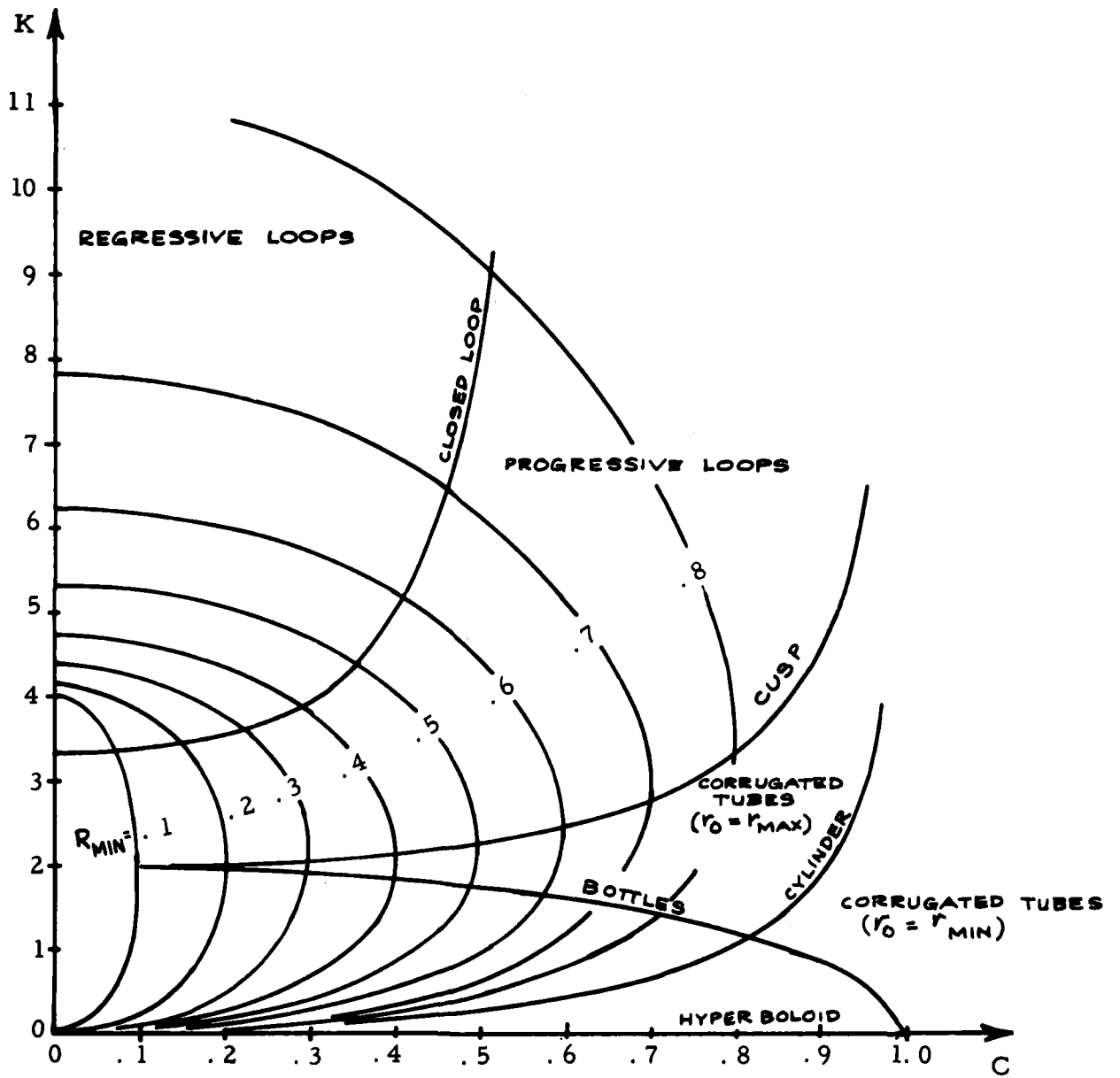


FIGURE 10-Isotensoid Domains In Function Of The Parameters C And K

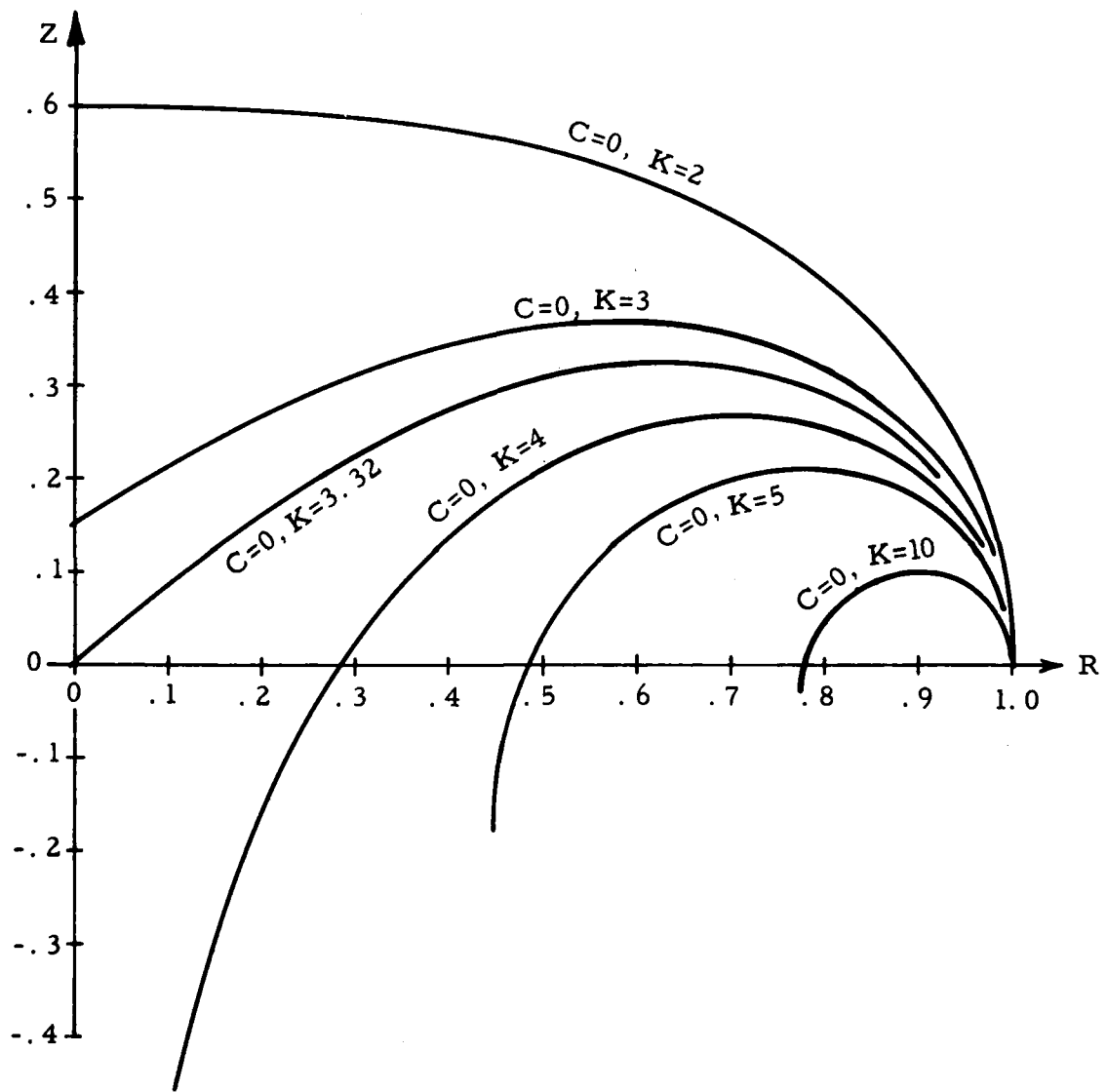


FIGURE 11-Isotensoid Shapes For C=0

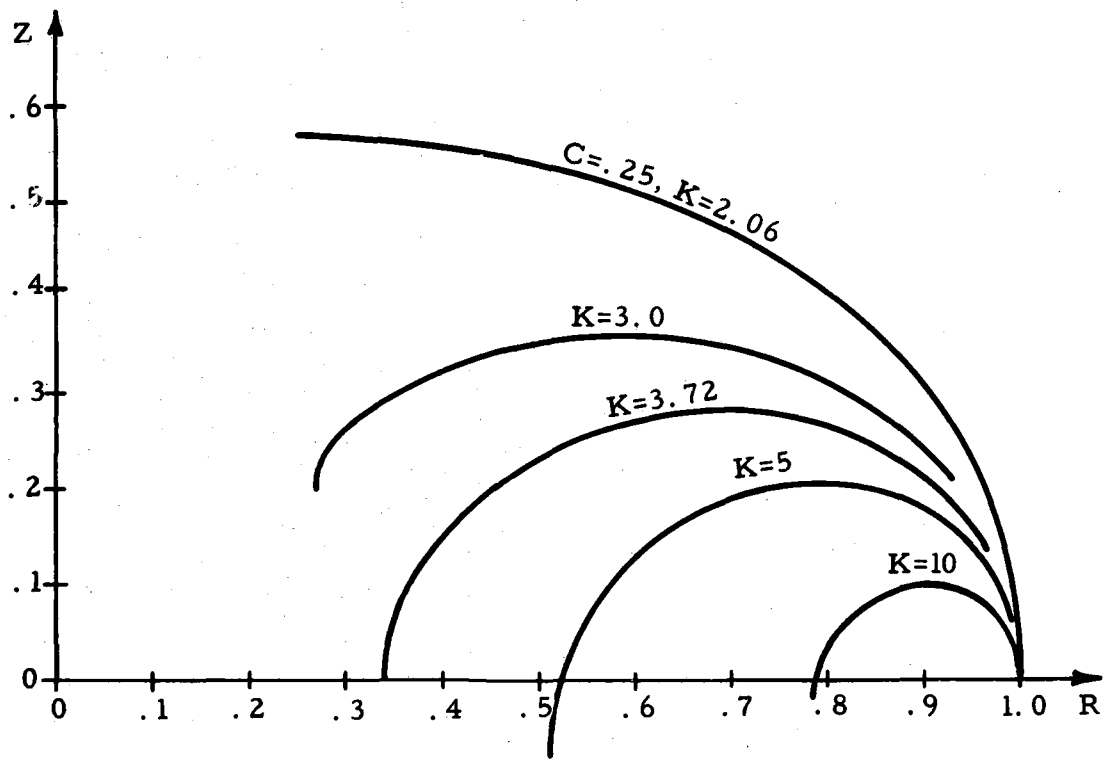


FIGURE 12-Isotensoid Shapes For $C = \frac{1}{4} .25$

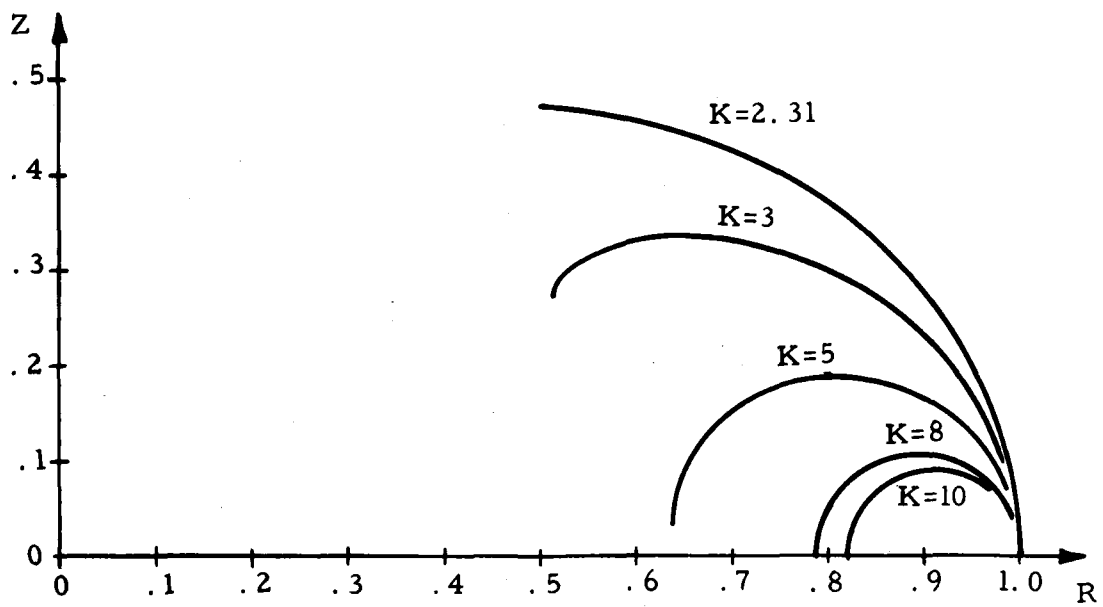


FIGURE 13-Isotensoid Shapes For $C = \pm .50$

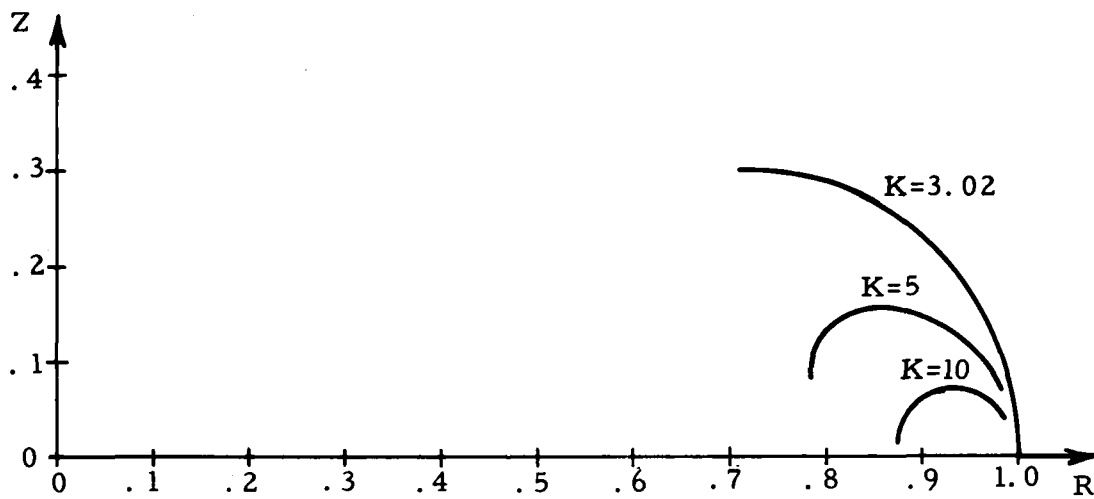


FIGURE 14-Isotensoid Shapes $C = \frac{1}{2} .75$

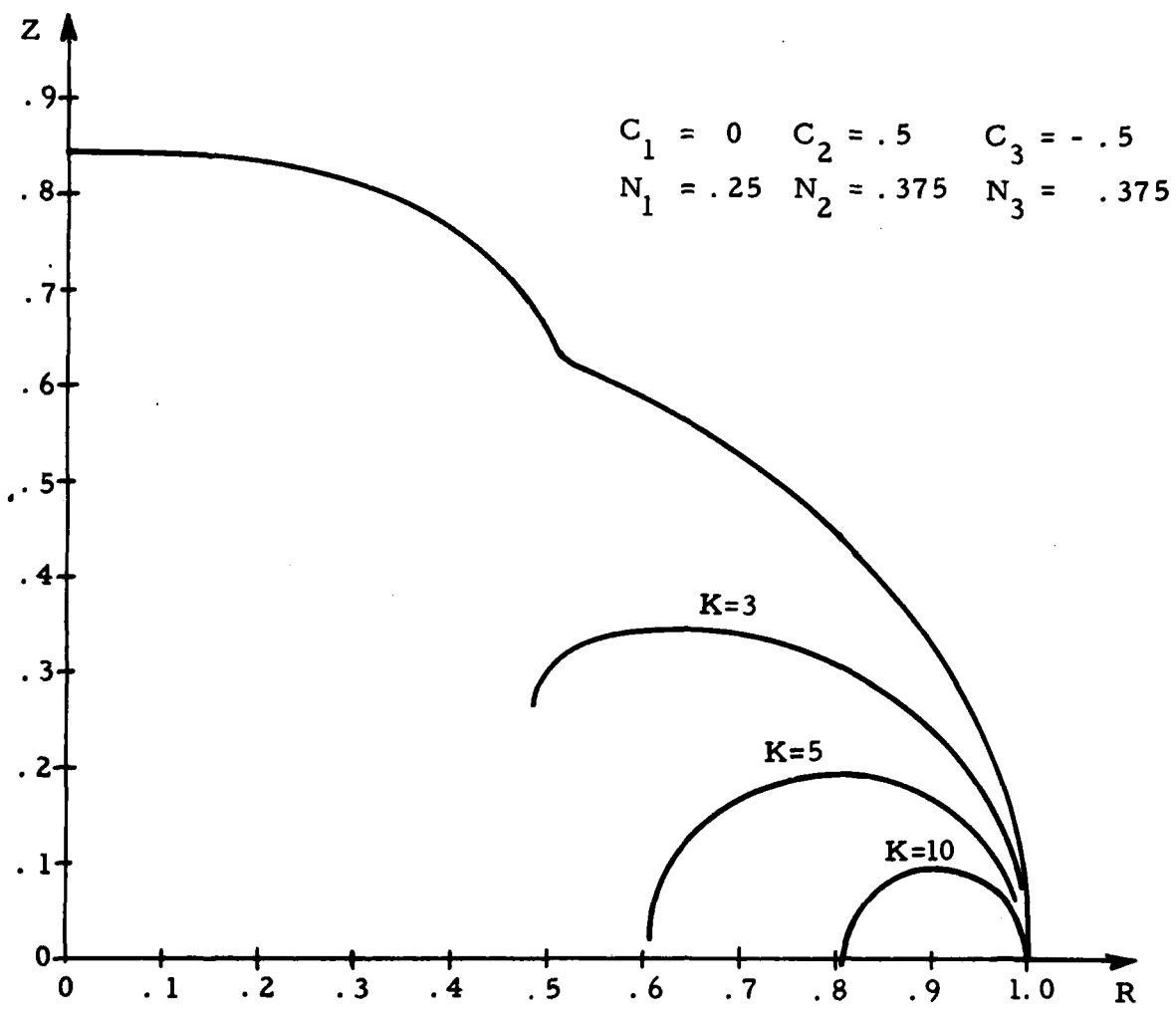


FIGURE 15-Isotenoid Shapes For Multiple Helix Angles

$C_1 = 0$	$C_2 = .5$	$C_3 = -.5$
$N_1 = .5$	$N_2 = .25$	$N_3 = .25$

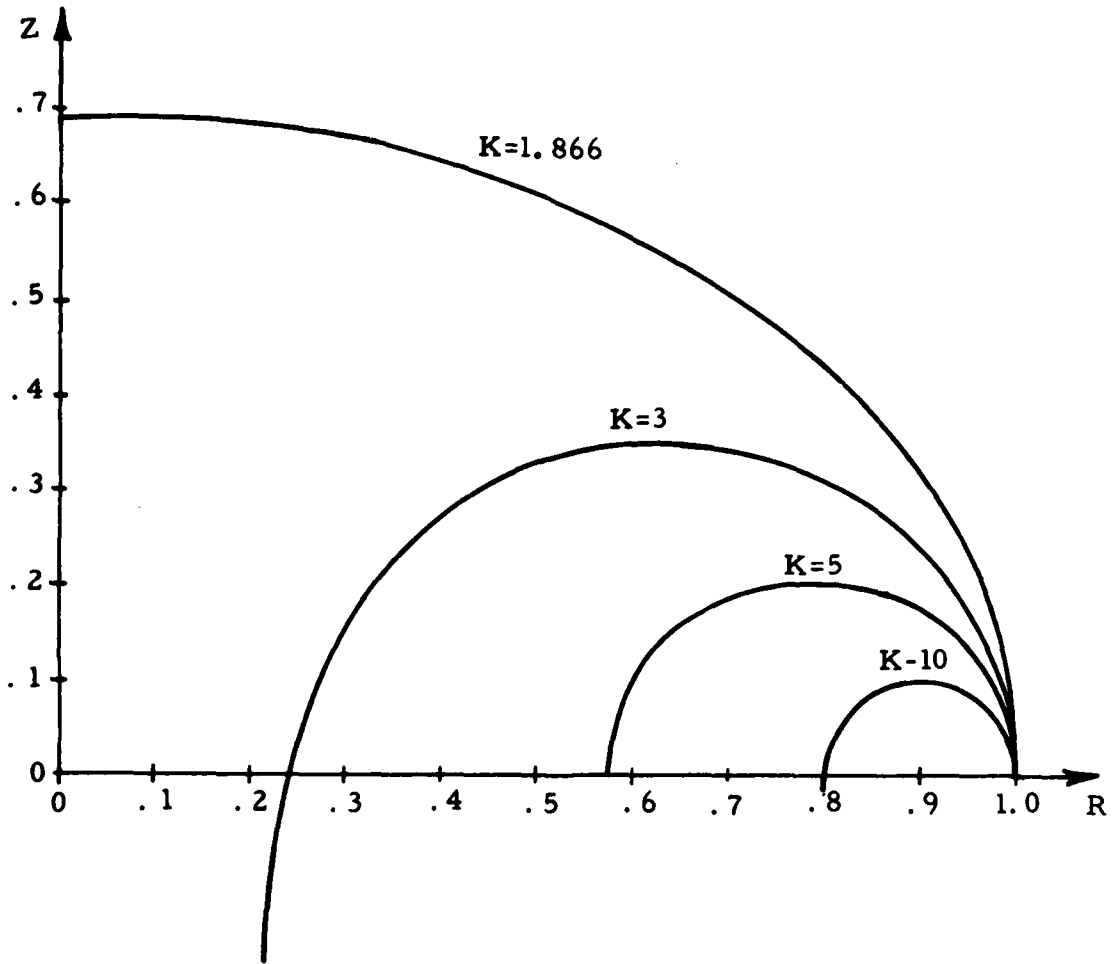


FIGURE 16-Isotensoid Shapes For Multiple Helix Angles

$C_1 = 0$	$C_2 = .5$	$C_3 = -.5$
$N_1 = .75$	$N_2 = .125$	$N_3 = .125$

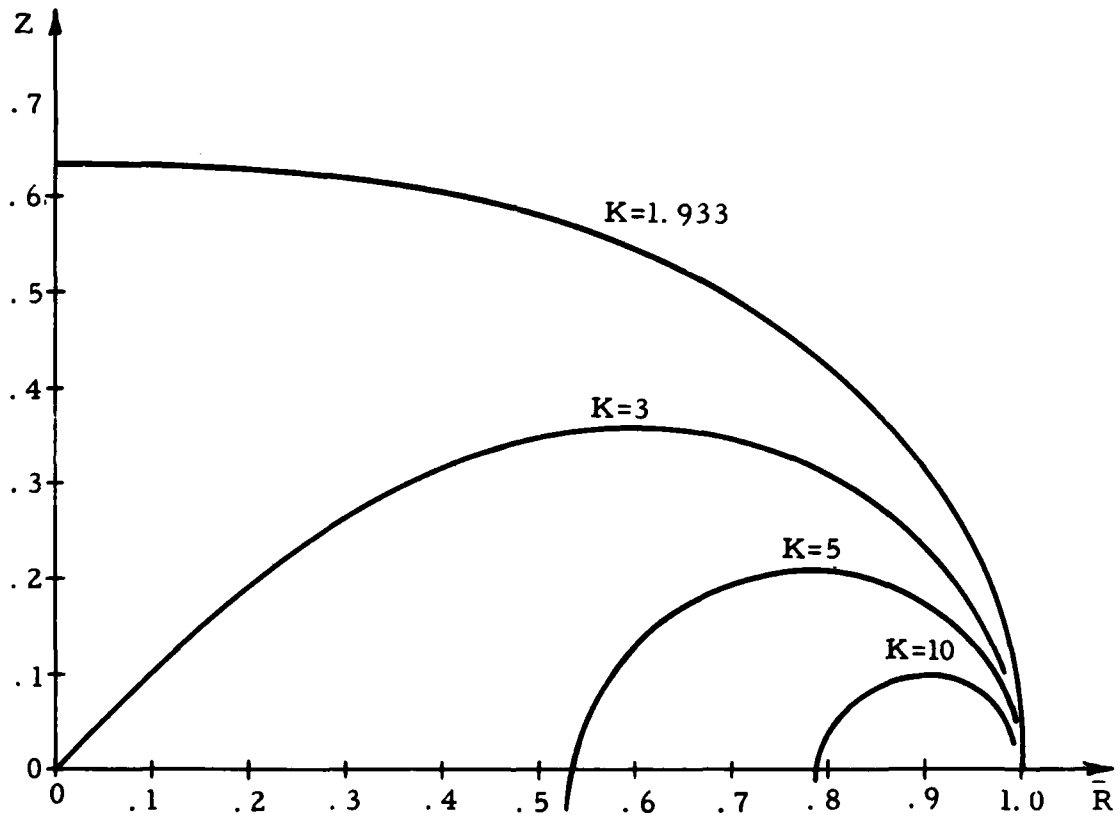


FIGURE 17-Isotenoid Shapes For Multiple Helix Angles

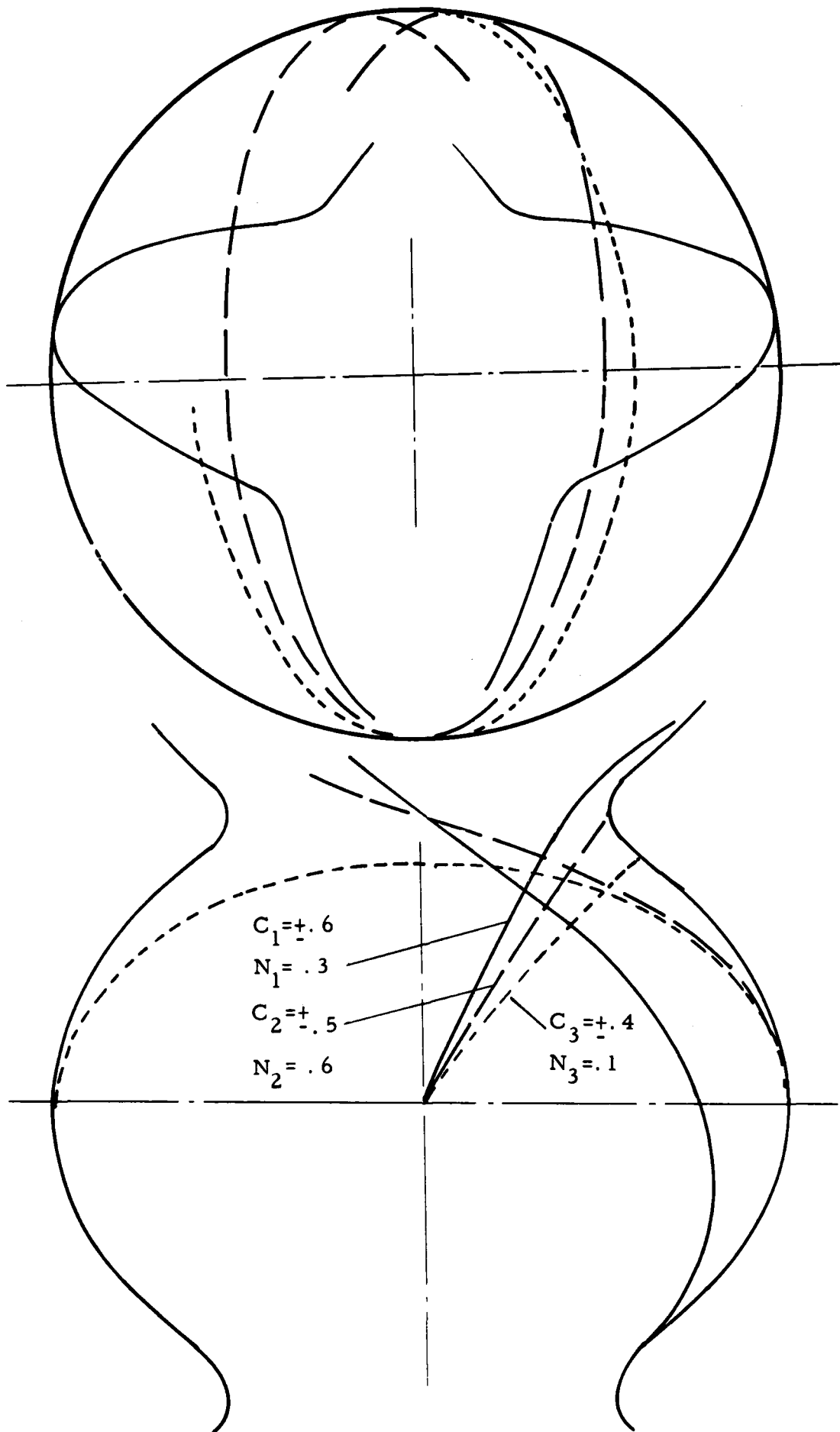


FIGURE 18- Schematic Of Isotensoid Shape And Fiber Geometry For Multiple Layered Corrugated Tube $K = 1.7$

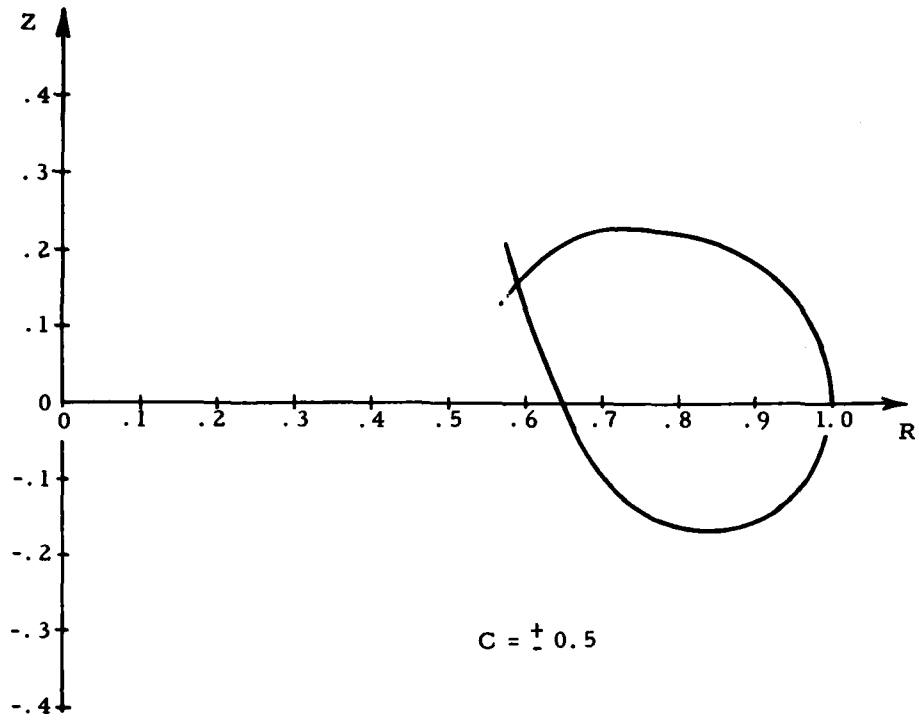


FIGURE 19-Isotenoid Shape For Linear Pressure Gradient

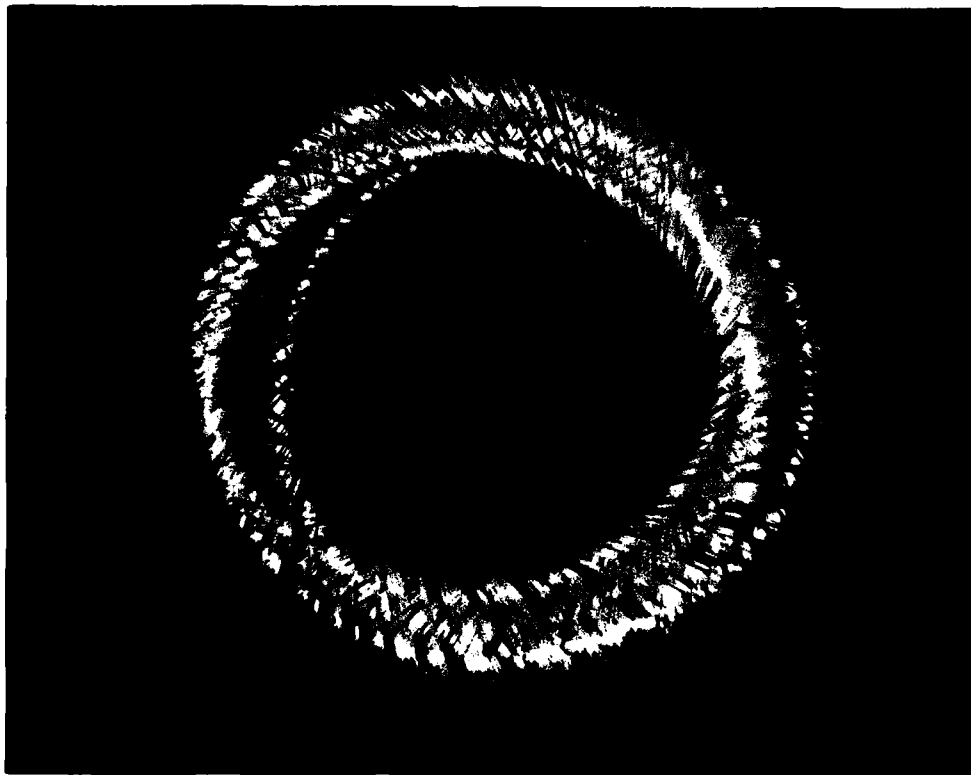


FIGURE 20-Isotenoid Shape And Filament Geometry For Closed Torus $C = \pm .35$ $K = 4.4$

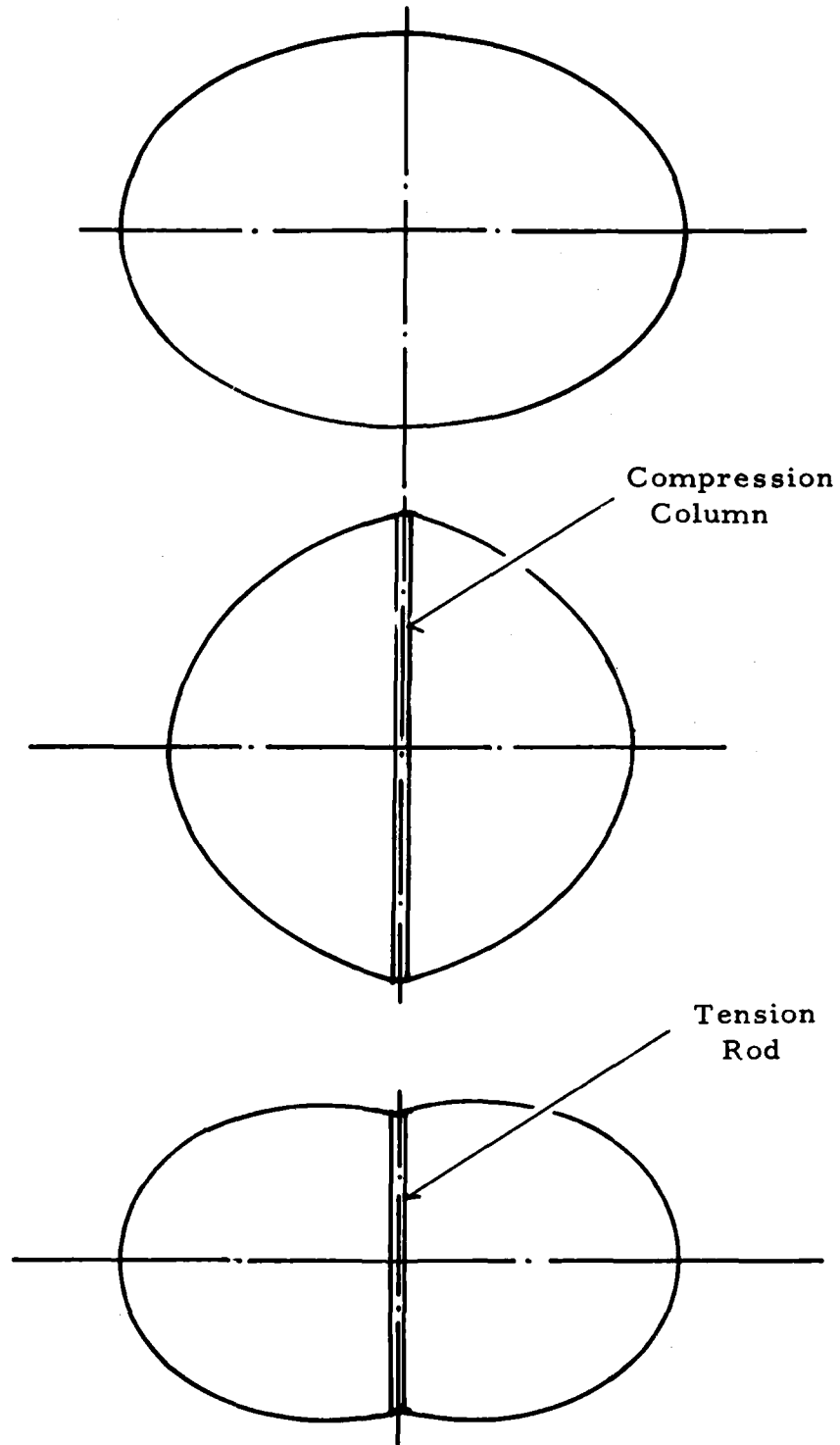


FIGURE 21-Closed Isotensoid Pressure Vessel-Type I

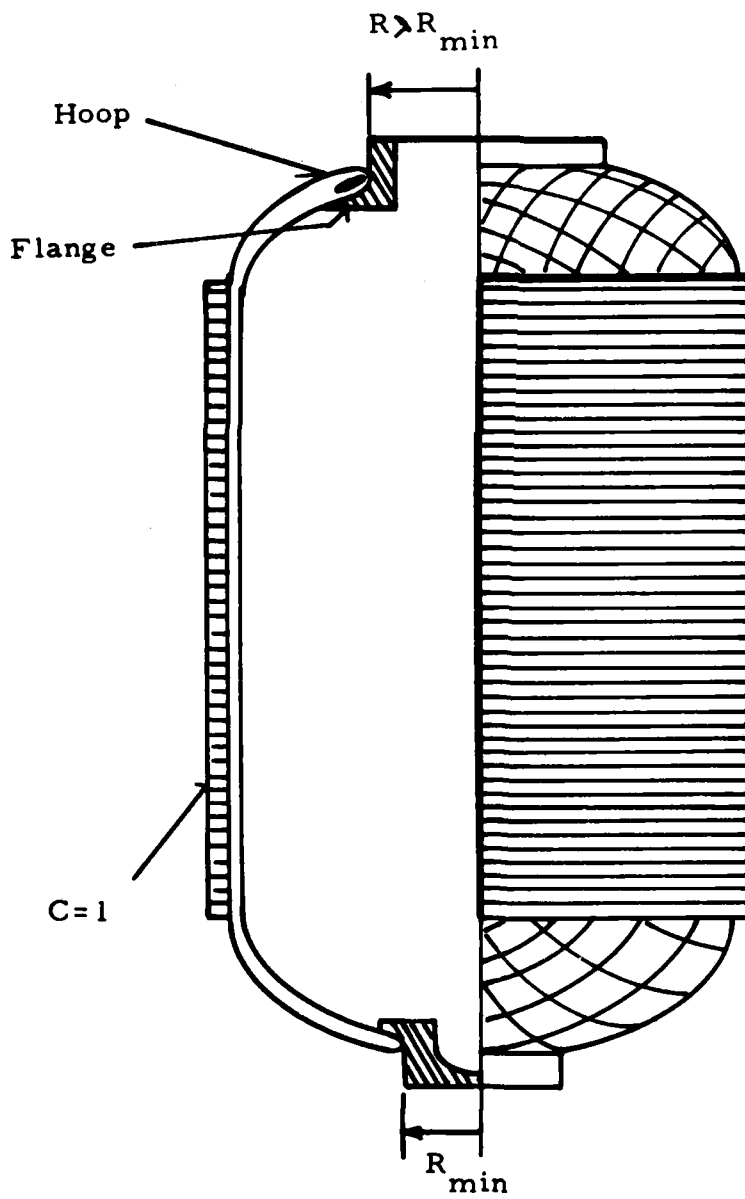


FIGURE 22-Closed Isotensoid Pressure Vessel-Type II

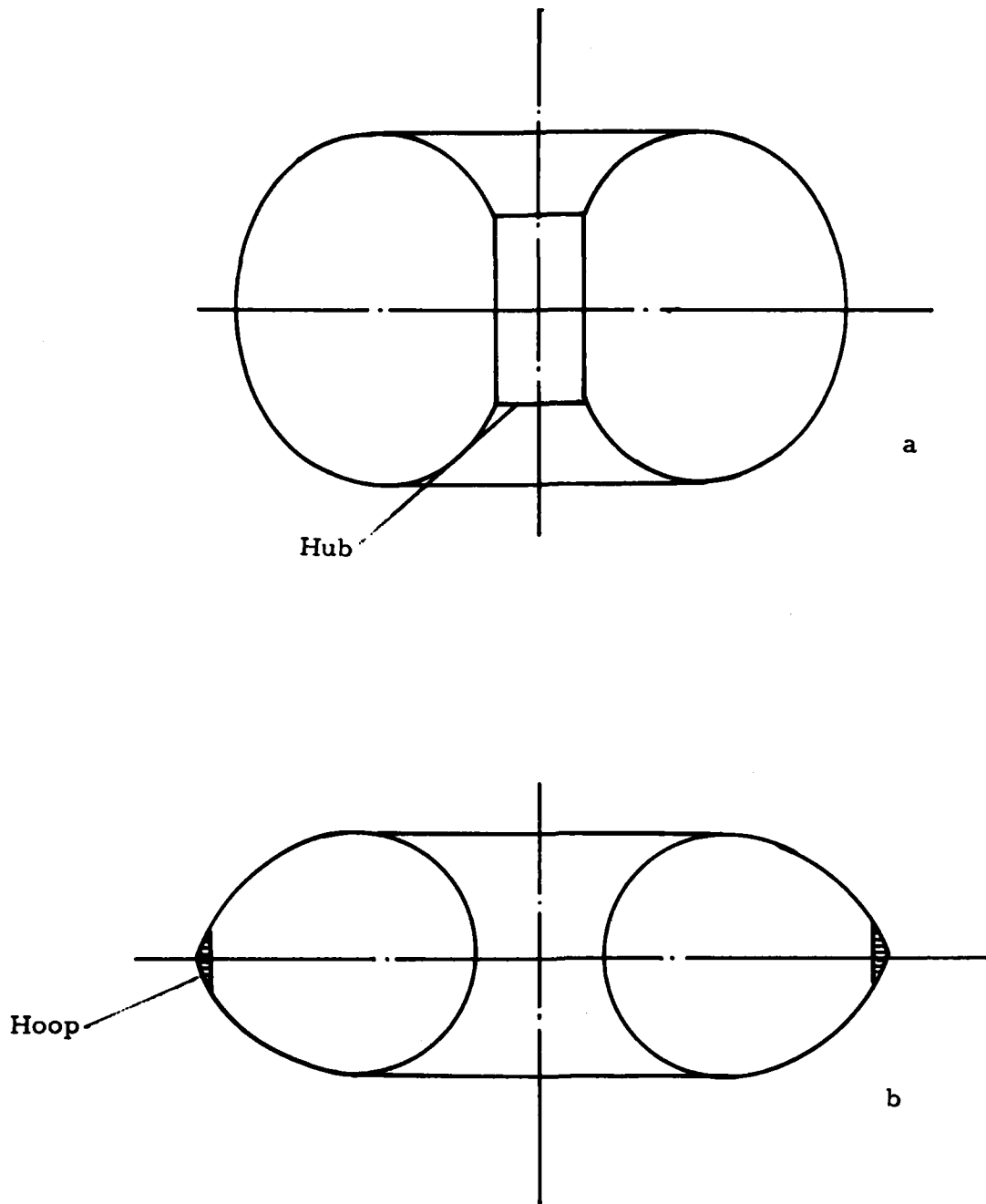


FIGURE 23-Closed Isotensoid Pressure Vessel-Type III

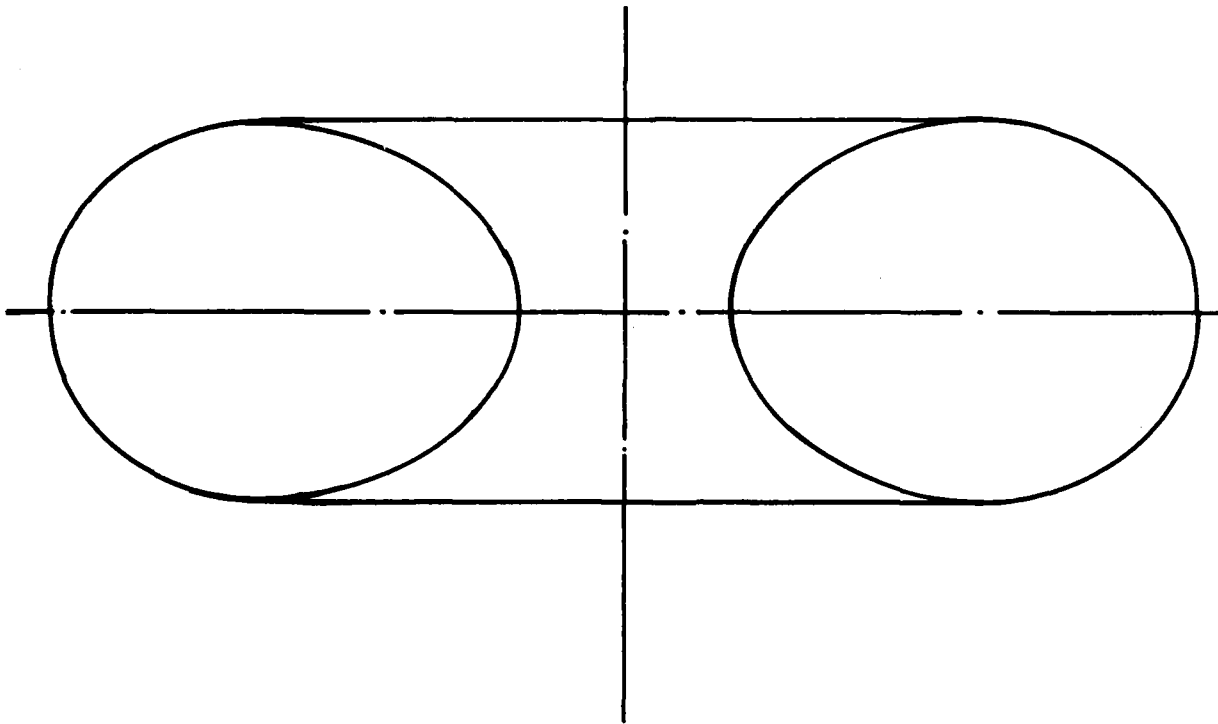


FIGURE 24-Closed Isotensoid Pressure Vessel-Type IV

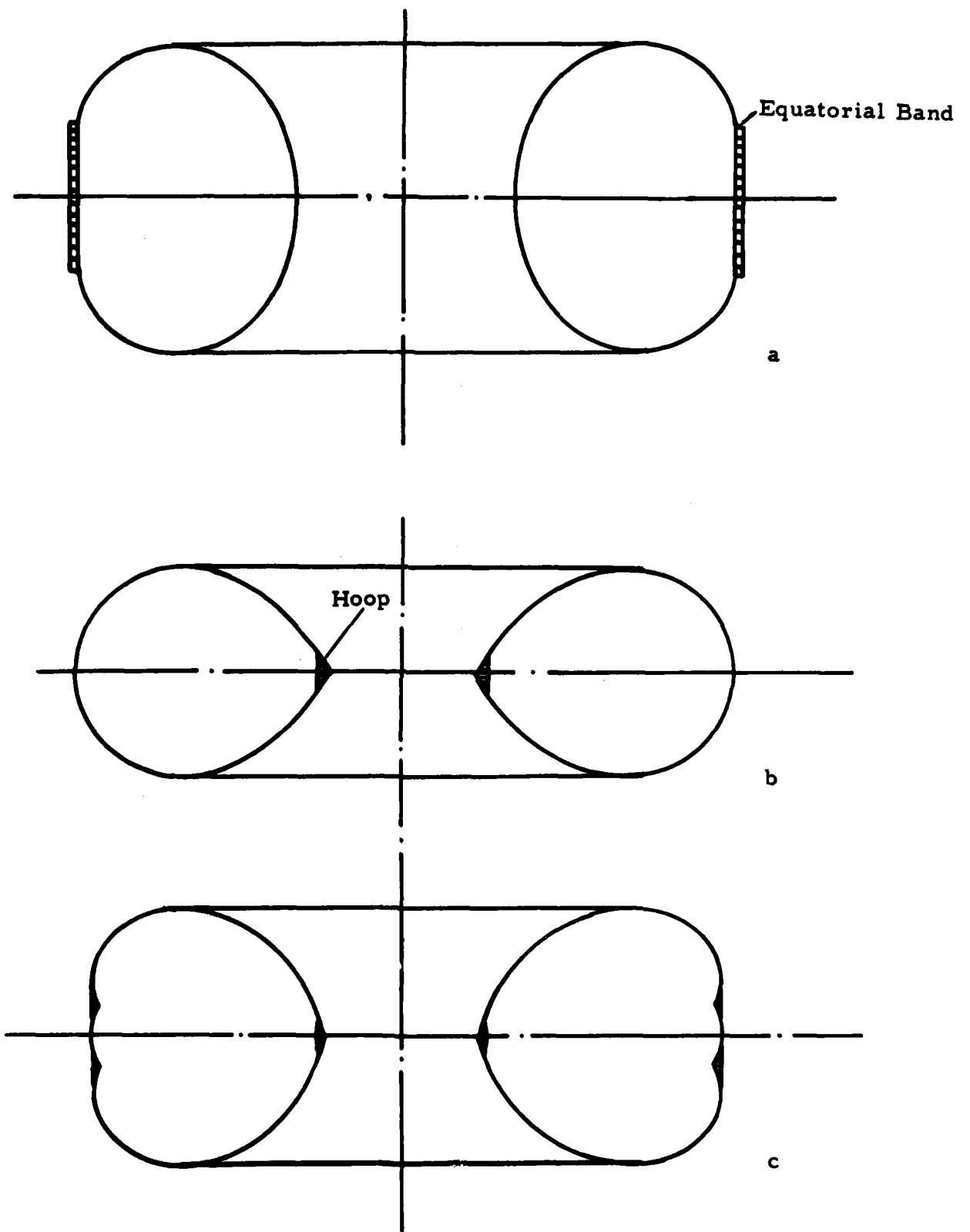


FIGURE 25-Closed Isotensoid Pressure Vessel-Type V

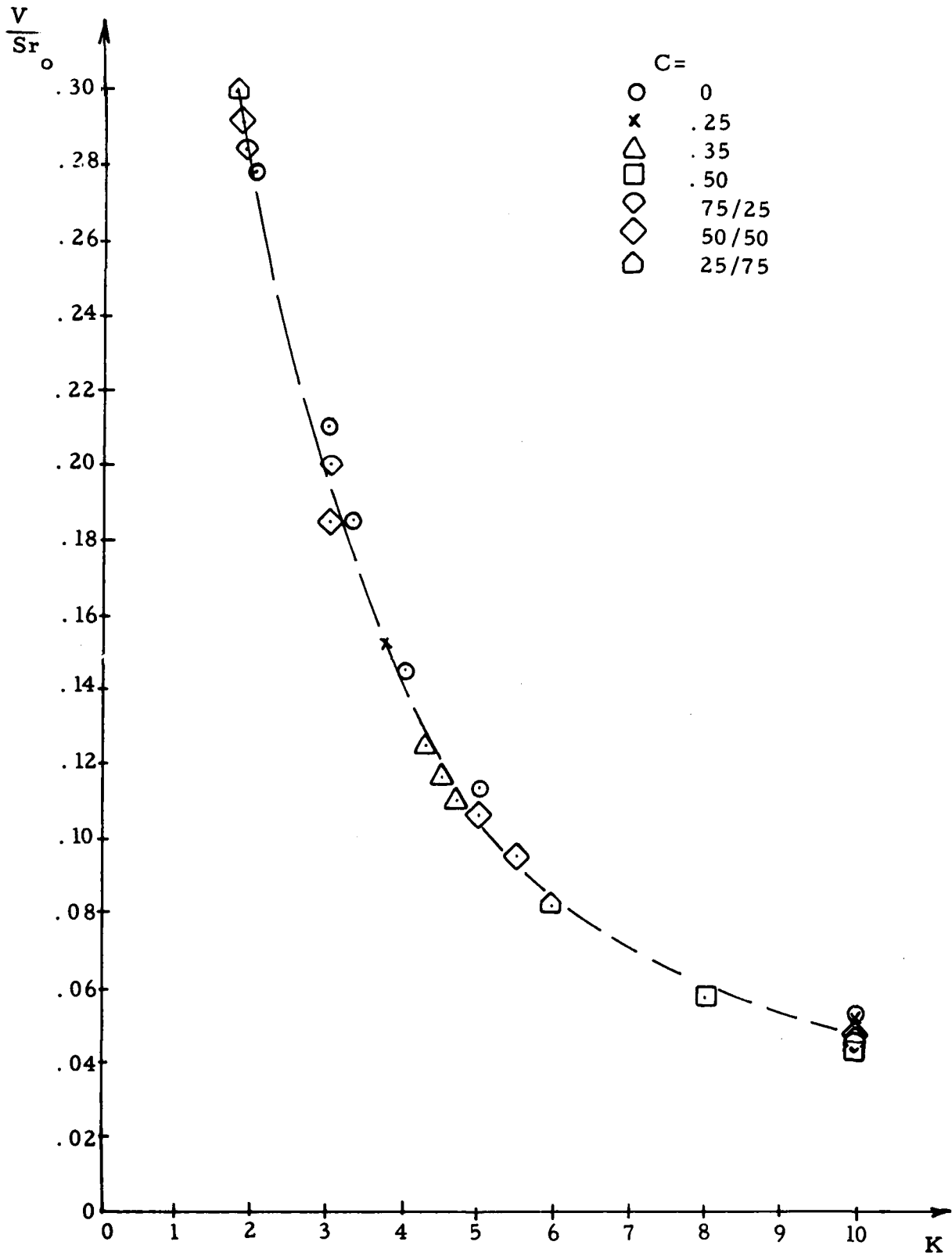


FIGURE 26-Non-dimensional Volume-Surface Ratio For Toroidal Isotenoid Pressure Vessels Of Type V-b

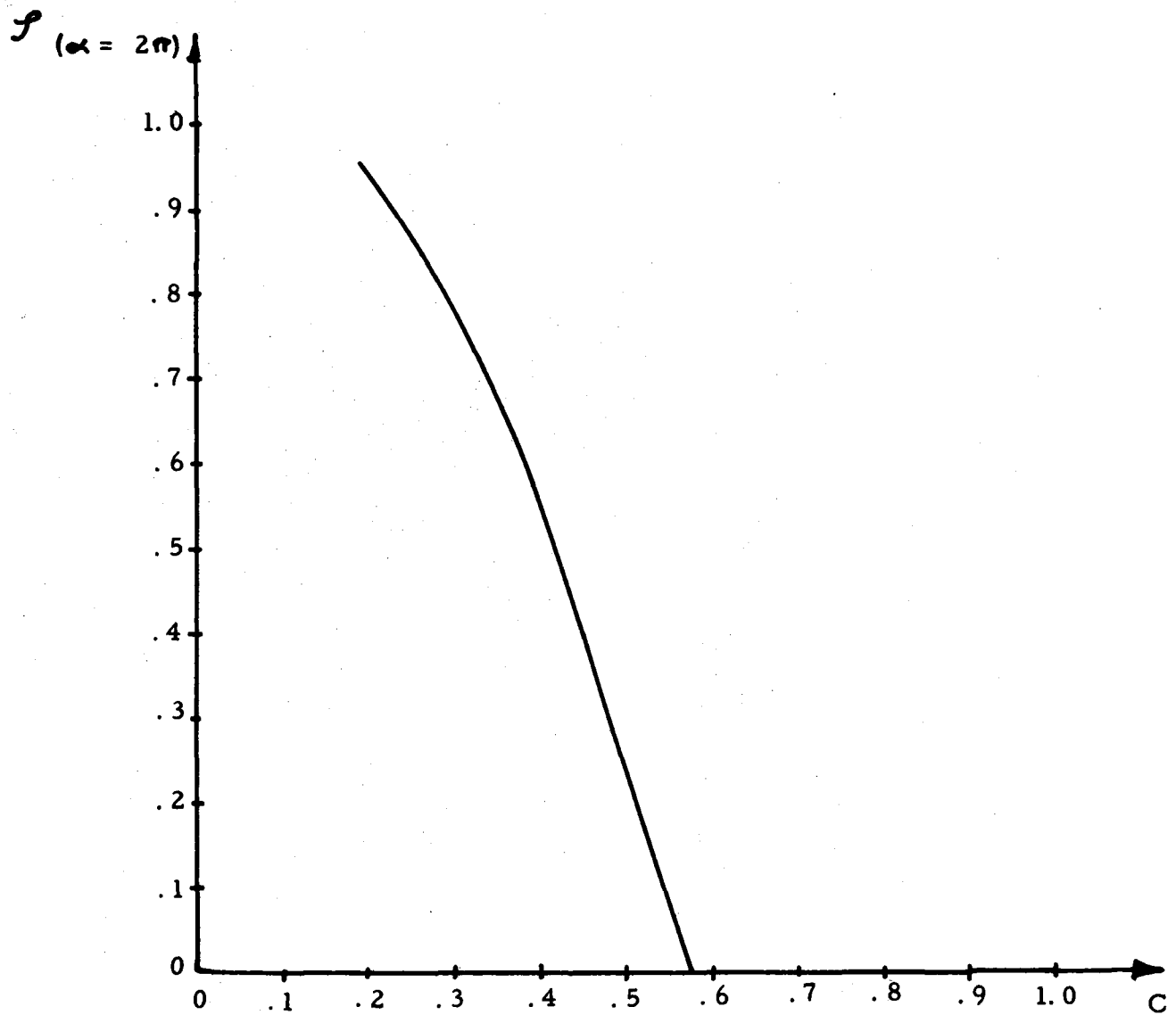


FIGURE 27-Central Angle f ($\alpha = 2\pi$) For Full Period Of Winding Pattern On Closed Toroidal Isotensoid Pressure Vessels Of Type IV

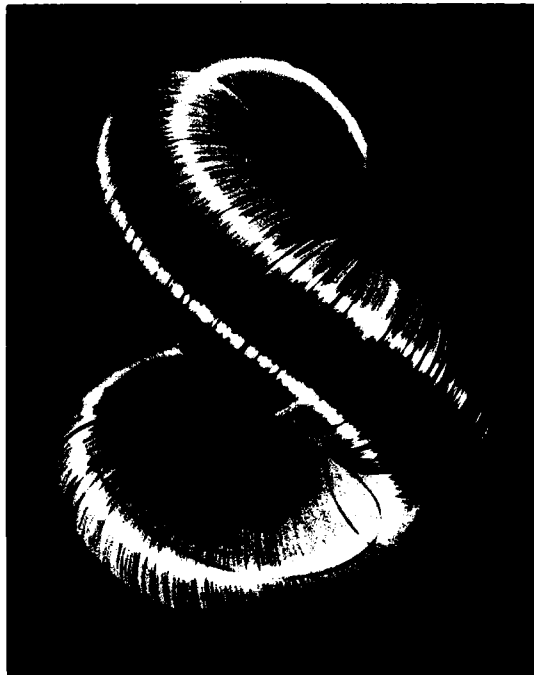


FIGURE 28 - Two-Lobed "Baseball Seam"
Instability Of Type V Toroidal Iso-
tensoid Pressure Vessel

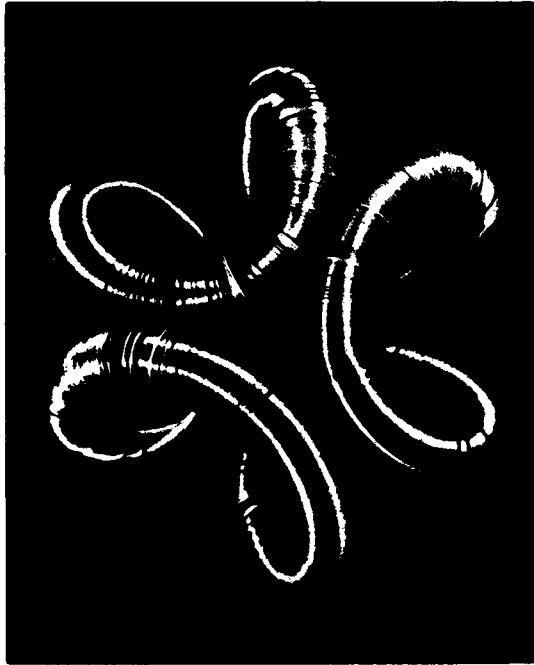


FIGURE 29 - Three-Lobed "Baseball Seam"
Instability Of Type V Toroidal Iso-
tensoid Pressure Vessel (Top View)



FIGURE 30 - Three-Lobed "Baseball Seam"
Instability Of Type V Toroidal Iso-
tensoid Pressure Vessel (Side View)



FIGURE 31 - "Python" Instability Of Type
V Toroidal Isotensoid
Pressure Vessel

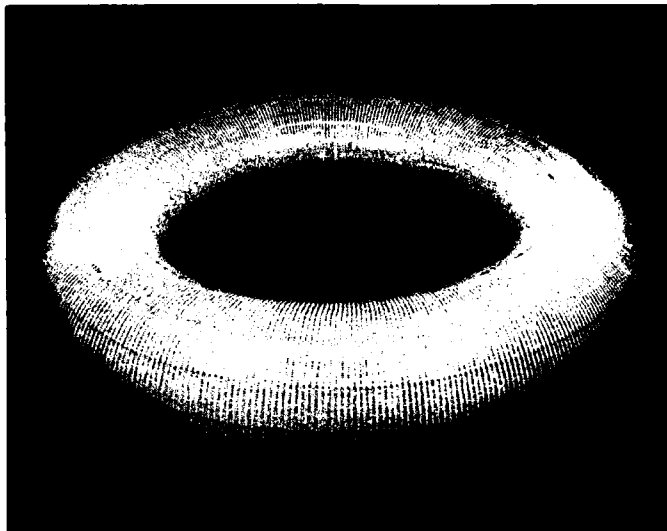


FIGURE 32-Knitted Toroid, Inflated

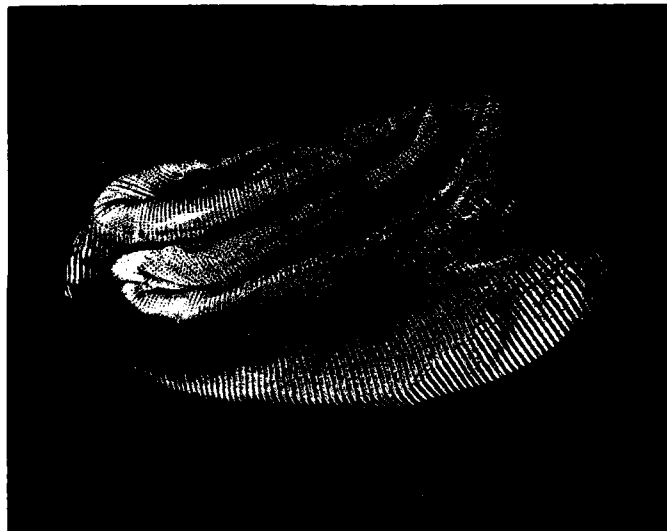


FIGURE 33-Knitted Toroid, Deflated and Folded

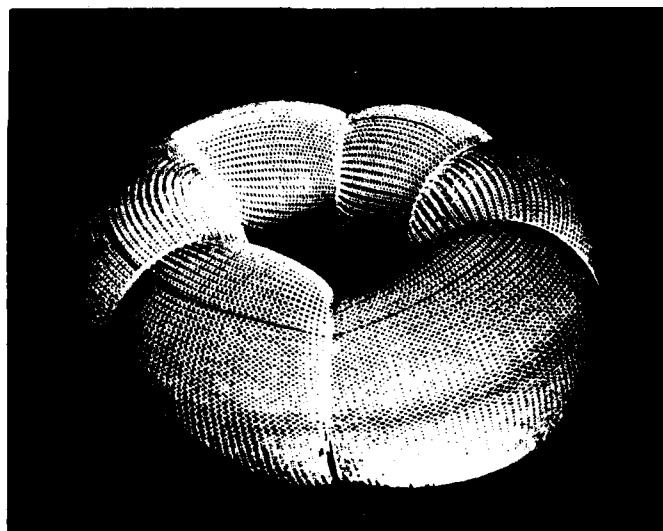


FIGURE 34-Corrugated Toroid, Knitted
And Filament-Wound

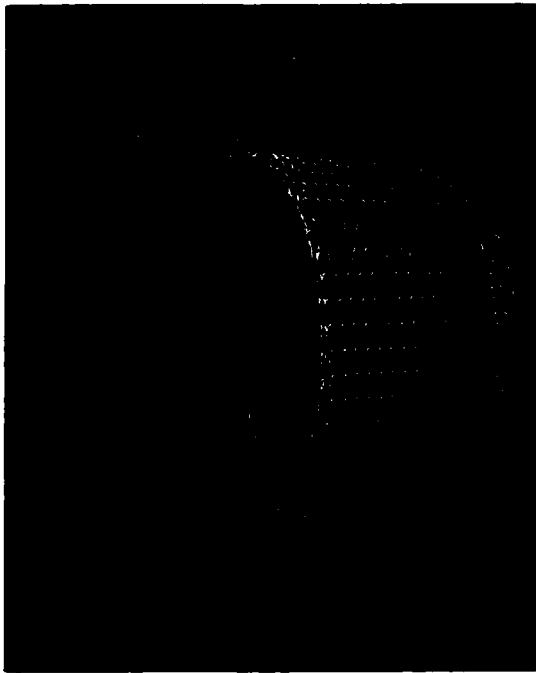


FIGURE 35-Meshed Tubular Structure
Made From Tungsten Wire
Straight Mesh Texture

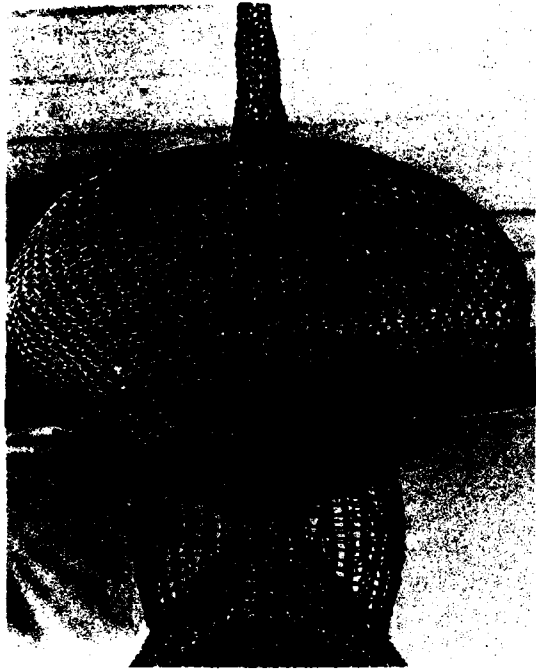


FIGURE 36-Meshed Interlacing Structure
Made From Brass Wire
Looped Mesh Texture

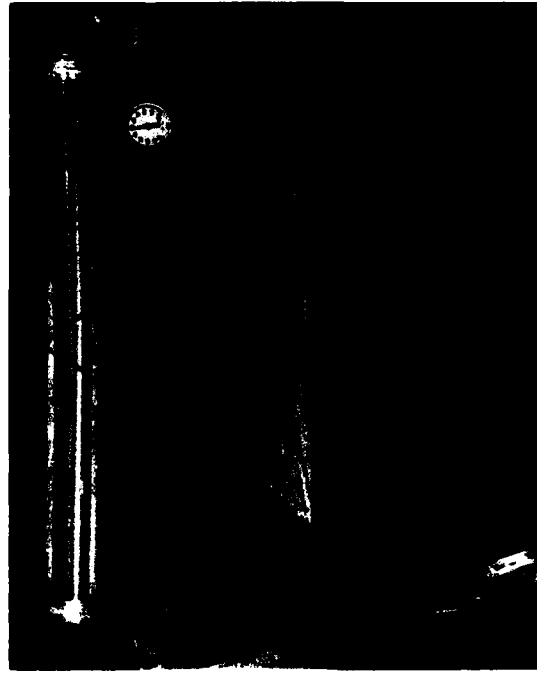


FIGURE 37-Isotensoid Pressure Vessel
Of Modified Type I,
Subject To Concentrated Side
Load

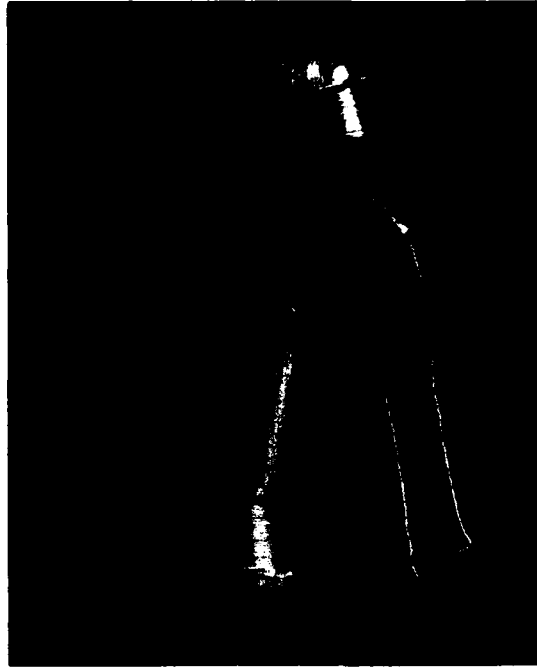


FIGURE 38-Isotensoid Pressure Vessel
Of Modified Type I,
Deflated And Folded